Experimental and Computational Investigation of Acetic Acid Deoxygenation over Oxophilic Molybdenum Carbide: Surface Chemistry and Active Site Identity

Joshua A. Schaidle[*,†], *Jeffrey Blackburn*[‡], *Carrie Farberow*[†], *Connor Nash*[†], *K. Xerxes Steirer*[#], *Jared Clark*[†], *David J. Robichaud*[†], *and Daniel A. Ruddy*[‡]

[†]National Bioenergy Center, [‡]Chemistry and Nanoscience Center, and [#]Materials Science Center, National Renewable Energy Laboratory, Golden, Colorado 80401, United States

ABSTRACT: *Ex-situ* catalytic fast pyrolysis (CFP) is a promising route for producing fungible biofuels; however, this process requires bifunctional catalysts that favor C-O bond cleavage, activate hydrogen at near atmospheric pressure and high temperature (350–500 °C), and are stable under high-steam, low hydrogen-to-carbon environments. Recently, early transition metal carbides have been reported to selectively cleave C-O bonds of alcohols, aldehydes, and oxygenated aromatics, yet there is limited understanding of the metal carbide surface chemistry under reaction conditions and the identity of the active sites for deoxygenation. In this paper we evaluated molybdenum carbide (Mo_2C) for the deoxygenation of acetic acid, an abundant component of biomass pyrolysis vapors, under *ex-situ* CFP conditions and probed the Mo_2C

Pursuant to the DOE Public Access Plan, this document represents the authors' peer-reviewed, accepted manuscript. The published version of the article is available from the relevant publisher.

surface chemistry, identity of the active sites, and deoxygenation pathways using *in-situ* diffuse reflectance infrared Fourier transform spectroscopy (DRIFTS), X-ray photoelectron spectroscopy (XPS), and density functional theory (DFT) calculations. The Mo_2C catalyst favored the production of acetaldehyde and ethylene from acetic acid over the temperature range of 250–400 °C, with decarbonylation pathways favored at temperatures greater than 400 °C. Little to no ethanol was observed due to the high activity of the carbide surface for alcohol dehydration. The Mo_2C surface, which was at least partially oxidized following pretreatment and exposure to reaction conditions (possibly existing as an oxycarbide), possessed both metallic-like H-adsorption sites (i.e., exposed Mo and C) and Brønsted acidic surface hydroxyl sites, in a ratio of 1:8 metallic:acidic sites following pretreatment. The strength of the acidic sites was similar to that for H-Beta, H-Y, and H-X zeolites. Oxygen vacancy sites (exposed Mo sites) were also present under reaction conditions, inferred from DRIFTS results and calculated surface phase diagrams. It is proposed that C-O bond cleavage steps proceeded over the acidic sites or over the oxygen vacancy sites and that the deoxygenation rate may be limited by the availability of adsorbed hydrogen, due to the high surface coverage of oxygen under reaction conditions. Importantly, the reaction conditions (temperature and partial pressures of H_2 and H_2O) had a strong effect on oxygen surface coverage, and accordingly, the relative concentrations of the different types of active sites, and could ultimately result in completely different reaction pathways under different reaction conditions.

KEYWORDS: Molybdenum carbide, acetic acid, deoxygenation, bio-oil, vapor phase upgrading, catalytic fast pyrolysis, oxygen vacancy, Brønsted acid

Pursuant to the DOE Public Access Plan, this document represents the authors' peer-reviewed, accepted manuscript. The published version of the article is available from the relevant publisher.

1. INTRODUCTION

Ex-situ catalytic fast pyrolysis (CFP) has been identified by the U.S. Department of Energy's Bioenergy Technologies Office as a promising route for the production of infrastructure-compatible, cost-competitive liquid hydrocarbon fuels from biomass.[1-4] This process seeks to reduce the severity and cost of downstream processing (e.g., hydrotreating) by adding a separate reactor in series with the fast pyrolysis unit to catalytically upgrade the biomass pyrolysis vapors prior to condensation. Consequently, catalysts that can operate effectively under *ex-situ* CFP conditions (vapor phase, 350–500 °C, near atmospheric pressure, high steam, low hydrogen-to-carbon, acidic), stabilize the resulting bio-oil, and enhance its fuel properties through hydrogenation, deoxygenation, and C-C coupling are required for the success of this biomass conversion pathway. In particular, these catalysts need to possess bifunctional properties (e.g., acidic and metallic sites), activate H_2 under low-pressure high-temperature conditions, and favor cleavage of C-O bonds over C-C bonds.[5]

Early transition metal carbides have been reported to possess bifunctional properties[6-9] and favor direct deoxygenation (DDO) and/or hydrodeoxygenation (HDO) reaction pathways (C-O cleavage) over decarbonylation and decarboxylation pathways (C-C cleavage).[9-18] Bej and Thompson demonstrated that Mo_2C produced primarily isopropanol and propylene from acetone and H_2 at 190–230 °C, via a sequential hydrogenation-dehydration pathway.[7] The authors proposed that hydrogenation occurred over metallic-like sites and dehydration occurred over acidic sites, demonstrated to be present on the Mo_2C surface by NH_3 temperature programmed desorption.[6,7] Similarly, other researchers have reported that olefins are the primary products from the conversion of C_2/C_3 alcohols and aldehydes over molybdenum and tungsten carbides in the presence of H_2.[9,11,12,14-16] Through O_2 co-feed and 2,6-di-tert-butylpyridine titrations, Sullivan

Pursuant to the DOE Public Access Plan, this document represents the authors' peer-reviewed, accepted manuscript. The published version of the article is available from the relevant publisher.

et al. experimentally demonstrated that Brønsted acidic sites were responsible for the dehydration of isopropanol to propylene at 140 °C over Mo_2C and that these sites were formed by interaction of oxygen with the Mo_2C surface (O*-Mo_2C).[9] High selectivity for the HDO of anisole to benzene at 147–247 °C and ambient pressure over Mo_2C catalysts has also been demonstrated.[17,18] The authors propose that two distinct types of sites are required for this HDO pathway and that the metallic sites (identity unknown) play a key role in the HDO chemistry.[17] Moreover, the density of available active sites on the Mo_2C surface was shown to decrease with increasing oxygen coverage (either from oxygen treatment or oxygenated reactants).[18] These studies illuminate the proclivity of oxophilic early transition metal carbides for deoxygenation reactions through selective C-O bond cleavage, and encourage further research to probe the surface chemistry and identity of the active sites under relevant reaction conditions as well as the dominant deoxygenation pathways.

Herein, we describe the characterization and evaluation of Mo_2C for the deoxygenation of acetic acid under conditions relevant to *ex-situ* CFP. Acetic acid was chosen as a model compound because (1) carboxylic acids comprise up to 25 wt% of pyrolysis vapors,[19] (2) these acids contribute significantly to the degradation and instability of bio-oils,[5] (3) acetic acid is the simplest carboxylic acid, and (4) it can undergo a variety of transformations allowing us to probe different reaction pathways. The primary reactions of acetic acid include decomposition (eqs 1–3), coupling (eq 4), dehydration (eq 5), and hydrogenation-dehydration (HDO) (eqs 6–8):

$CH_3COOH \rightarrow 2\ CO + 2\ H_2$	Gasification	(1)
$CH_3COOH + H_2 \rightarrow CO + CH_4 + H_2O$	Decarbonylation	(2)
$CH_3COOH \rightarrow CO_2 + CH_4$	Decarboxylation	(3)
$2\ CH_3COOH \rightarrow (CH_3)_2CO + CO_2 + H_2O$	Ketonization	(4)

Pursuant to the DOE Public Access Plan, this document represents the authors' peer-reviewed, accepted manuscript. The published version of the article is available from the relevant publisher.

$CH_3COOH \rightarrow 2\ C + 2\ H_2O$ Dehydration (5)

$CH_3COOH + H_2 \rightarrow CH_3CHO + H_2O$ Hydrogenation-dehydration (6)

$CH_3COOH + 2\ H_2 \rightarrow CH_3CH_2OH + H_2O$ Hydrogenation-dehydration (7)

$CH_3COOH + 2\ H_2 \rightarrow C_2H_4 + 2\ H_2O$ Hydrogenation-dehydration (8)

The catalytic properties of Mo_2C were tested for acetic acid deoxygenation using a temperature programmed reaction (TPRxn). TPRxn experiments with ethanol and acetaldehyde (possible reaction intermediates) as the feed were also performed to elucidate deoxygenation pathways. The surface chemistry of Mo_2C was investigated using *in-situ* diffuse reflectance infrared Fourier transform spectroscopy (DRIFTS) and X-ray photoelectron spectroscopy (XPS) coupled with density functional theory (DFT) calculations. The results provide insight into the preferred reaction pathway(s) and the identity of the active site(s), and highlight the need to balance the rates of hydrogenation and dehydration over early transition metal carbide materials in order to further enhance performance.

2. EXPERIMENTAL SECTION

2.1. Catalyst Preparation

The Mo_2C catalyst was synthesized using a temperature-programmed reaction procedure.[20-22] 5 g of ammonium paramolybdate (AM, $(NH_4)_6Mo_7O_{24} \bullet 4H_2O$, Alpha-Aesar, sieved to 125 – 250μm) was loaded into a quartz tube reactor on top of a quartz wool plug. The AM was reduced and carburized in 15% CH_4/H_2 flowing at 1200 mL/min. The sample temperature was increased from room temperature (RT) to 200 °C at 10 °C/min, followed by heating from 200 to 590 °C at 1 °C/min. The sample remained at 590 °C for 2 h before quenching to RT. The resulting material

Pursuant to the DOE Public Access Plan, this document represents the authors' peer-reviewed, accepted manuscript. The published version of the article is available from the relevant publisher.

was passivated using a 1% O_2/He mixture flowing at 20 mL/min for 12 h, and was then stored under a nitrogen atmosphere until use.

2.2. Catalyst Characterization

2.2.1. X-ray Diffraction

Powder X-ray diffraction (XRD) data were collected using a Rigaku Ultima IV diffractometer with a Cu Kα source. Diffractograms were collected in the 2θ range of 20 – 80 degrees at a scan rate of 2 °/min. The Mo_2C sample (ca. 20 mg) was supported on a glass sample holder with a 0.2 mm recessed sample area and was pressed into the recession with a glass slide to obtain a uniform z-axis height.

2.2.2. Surface Area Measurements

Nitrogen physisorption data were collected at 77 K using a Quantachrome Quadrasorb SI instrument. The Mo_2C sample was pre-treated under vacuum for 2 h at 150 °C. Surface area was determined using the Brunauer-Emmett-Teller (BET) method, and pore volume was determined from the adsorption isotherm data using the Barrett-Joyner-Halenda (BJH) method.

2.2.3. H_2 Chemisorption

The density ($\mu mol/g_{cat}$) of H-adsorption sites was measured from chemisorbed H_2 isotherms collected at 40 °C (P/P_0 80-560 mmHg) using a Quantachrome Autosorb 1-C. The Mo_2C sample was reduced *in-situ* at 400 °C, then evacuated at 400 °C for 2 h. H-adsorption site density was calculated from the combined isotherm using a 1:1 H:metal atom stoichiometry.

Pursuant to the DOE Public Access Plan, this document represents the authors' peer-reviewed, accepted manuscript. The published version of the article is available from the relevant publisher.

2.2.4. Total Acid Site Titration: NH_3 Temperature Programmed Desorption

The total number of acid sites on the Mo_2C catalyst was determined by temperature programmed desorption of ammonia (NH_3-TPD). The catalyst sample (ca. 200 mg) was loaded into a ½" quartz U-tube reactor and analyzed using a dedicated micro-flow reactor system (Altamira's AMI-390) equipped with a thermal conductivity detector (TCD). The sample was reduced in 25 mL/min of 10% H_2/Ar by heating at 10 °C/min from room temperature to 400 °C. The final reduction temperature was maintained for 2 h. The sample was then cooled to 80 °C in flowing He, and saturated with 10% NH_3/He flowing at 25 mL/min for 2 h. Excess and/or physisorbed NH_3 was removed by holding the sample at 80 °C for 10 min in flowing He. NH_3-TPD was performed by heating the catalyst from 80 °C to 650 °C at 20 °C/min in flowing He (25 mL/min), followed by a 10 min hold at 650 °C. A sample loop of known volume (500 μL) was used to calibrate the TCD response for 10% NH_3/He and quantify the amount of NH_3 desorbed from the catalyst sample. Surface acidic sites were quantified by assuming adsorption stoichiometry of one NH_3 molecule adsorbed per acid site.

2.2.5. X-ray Photoelectron Spectroscopy

The as-prepared, pretreated, and spent Mo_2C catalysts were characterized using X-ray photoelectron spectroscopy (XPS) to determine the compositions and oxidation states of species on the surfaces. Following various treatments, Mo_2C samples were removed from the reactor without air exposure and transferred to an Ar atmosphere glove box. Samples were prepared in the glove box by pressing catalyst powders onto indium foil, then attaching the foil to the sample holder with conductive carbon tape. XPS experiments were performed using a Physical Electronics (PHI) 5600 photoelectron spectrometer equipped with a glove box for loading samples. Excitation was provided with an Al anode (Kα radiation at 1486.6 eV) operating at 25

Pursuant to the DOE Public Access Plan, this document represents the authors' peer-reviewed, accepted manuscript. The published version of the article is available from the relevant publisher.

mA and 15 kV. Core level spectra were collected for carbon (C 1s), molybdenum (Mo 3d), and oxygen (O 1s) at an analyzer pass energy of 11.75 eV. Binding energies were calibrated by comparing centroid positions of clean Cu $2p_{3/2}$, Ag $3d_{5/2}$, and Au $4f_{7/2}$ from measured and accepted values.[23] The spectra were deconvoluted using a nonlinear least squares method employing a combination of Gaussian (80%) and Lorentzian (20%) distributions in Multipak, a commercially available XPS analysis program. Shirley backgrounds were applied to O 1s and Mo 3d spectra, whereas the decreasing background in the C 1s region required a linear background subtraction. No charging of the samples was observed. Parameter constraints were imposed during deconvolution of the Mo spectra. The Mo 3d spectra were fit using doublets with a splitting of 3.18 eV between the $3d_{5/2}$ and $3d_{3/2}$ peaks and an intensity ratio of 3:2. For all spectra, the peak widths (i.e., full width half maximum, FWHM) for the doublets were constrained to be similar. Peak areas were normalized using the appropriate atomic sensitivity factors and instrument transmission function provided in Multipak. This allowed comparison of the relative atomic fractions of each species on the catalyst surfaces.

2.3. Temperature Programmed Reaction

Temperature programmed reaction (TPRxn) experiments were performed in a micro-reactor system, equipped with a bubbler for introduction of vapors and a mass spectrometer (RGA 100, Stanford Research Systems) for analysis of the reactor effluent. He and H_2 were introduced into the system through MKS mass flow controllers. Approximately 50 mg of catalyst was loaded into the quartz u-tube reactor and supported on quartz wool. Prior to TPRxn experiments, the Mo_2C catalysts were reduced in 20% H_2/He at 50 mL/min for 2 h at 400 °C (5 °C/min heating rate). The reduction temperature was selected based on a H_2 temperature programmed reduction experiment (Figure S1).

Pursuant to the DOE Public Access Plan, this document represents the authors' peer-reviewed, accepted manuscript. The published version of the article is available from the relevant publisher.

Following reduction, the catalyst was cooled to RT in flowing He and then exposed to the reaction mixture consisting of 1.5 mol% acetic acid, 5.8 mol% H_2, and 92.7% He (ca. 43.2 mL/min total flow, H_2/acetic acid molar ratio of ca. 3.8). After the mass spectrometer signal stabilized, the temperature was increased from RT to 600 °C at 10 °C/min. Similar experiments were also performed with ethanol and acetaldehyde in place of acetic acid. The feed mixtures were 5.8 mol% ethanol, 5.5 mol% H_2, and 88.7% He (ca. 45.1 mL/min total flow, H_2/ethanol molar ratio of ca. 1) and 2.2 mol% acetaldehyde, 5.7 mol% H_2, and 92.1% He (ca. 43.5 mL/min total flow, H_2/acetaldehyde molar ratio of ca. 2.6). To achieve these mixtures, the bubbler was maintained at RT for acetic acid and ethanol and -50 °C for acetaldehyde using a 50:50 by volume mixture of ethanol and ethylene glycol with dry ice as the cooling agent.[24] The H_2/organic reactant molar ratios were chosen to achieve approximately the stoichiometric amount of H_2 required for complete saturation and deoxygenation of the organic molecule, with the final product being ethane (e.g., ethanol conversion to ethane requires one H_2 molecule, and the selected molar ratio of H_2/ethanol was ca. 1). All experiments were performed at atmospheric pressure. Mass spectra were deconvoluted using a method adapted from Ko et al.[25] and Zhang et al.[26] A full description of the deconvolution method and equations for calculating conversion and reactant consumption rates are provided in the Supporting Information and Tables S1 and S2.

2.4. *In-situ* DRIFTS

DRIFTS measurements were performed on a Thermo-Nicolet 6700 FTIR spectrometer fit with a Harrick “Praying Mantis” high pressure/high temperature DRIFTS cell. The DRIFTS spectra displayed in this manuscript were acquired using 256 scans for both the background and the sample scan. All spectra shown were baseline-corrected to remove any gradual sloping changes in the spectral baseline.

Pursuant to the DOE Public Access Plan, this document represents the authors' peer-reviewed, accepted manuscript. The published version of the article is available from the relevant publisher.

Two general types of Mo_2C samples were studied in the DRIFTS measurements. The first sample was the as-prepared Mo_2C, which was not diluted with KBr. Such samples are most useful for identifying gas-phase products, since the total penetration depth of the IR probe beam is low, but the moles of evolved gas-phase products is as high as possible. The other sample is a dilution of ca. 1:20 (by weight) Mo_2C:KBr. These samples enable deeper penetration depth of the IR probe beam into the sample cup, and provide high signal-to-noise for species adsorbed to the Mo_2C surface. Samples were handled in air prior to measurement, and were loaded into the DRIFTS sample cup in air.

All samples were first reduced in pure flowing hydrogen (or deuterium in some cases). The H_2 or D_2 flow rate was held at 200 mL/min, and the total pressure was held at 500 Torr. The sample temperature was ramped in the flowing H_2 environment at a rate of 5 °C/min to 400 °C, and held at 400 °C for 5 to 30 min. After the H_2 reduction, samples were exposed to acetic acid vapor by bubbling argon gas (500 mL/min, 500 Torr total pressure) through an acetic acid bubbler for times ranging from 10 min to 1 h. Isotope experiments utilized deuterated acetic acid (CH_3COOD) or ^{13}C-labeled acetic acid ($CH_3{}^{13}COOH$) in lieu of natural acetic acid (CH_3COOH). After acetic acid exposure, the sample chamber was evacuated for times ranging from several hours to overnight, depending on the experiment. Temperature-programmed DRIFTS reaction experiments were then performed by increasing the temperature to 400 °C (ramp rate of 5 °C/min) in different environments. Three environments were explored for observing acetic acid desorption, decomposition, and reaction: vacuum, flowing Ar, and flowing 4% H_2 in Ar. The flow rate was 200 mL/min, with a constant pressure of 500 Torr, for all flowing gas environments.

Pursuant to the DOE Public Access Plan, this document represents the authors' peer-reviewed, accepted manuscript. The published version of the article is available from the relevant publisher.

2.5. Computational Details

All calculations used Kohn-Sham density function theory solved using a plane-wave basis set as implemented in the Vienna Ab initio Simulation Package (VASP).[27-30] The ion-electron interactions were described using PAW potentials[31,32] with an energy cutoff of 400 eV. The generalized gradient corrected PBE exchange-correlation functional[33,34] was used for all calculations. All calculations included spin-polarization and dispersion corrections as developed by Tkatchenko-Scheffler (DFT-TS).[35] Optimizations were considered complete when forces fell below 0.05 eV/Å. The surface Brillouin zone was sampled using a 5 × 5 × 1 Monkhorst–Pack mesh[36] and a Methfessel−Paxton smearing of 0.2 eV; all energies reported are at zero broadening. Molecules in the gas phase were studied using a 13 × 14 × 15 $Å^3$ unit cell. During optimization, all of the relevant adsorbed species and the top ½ layers of each surface are allowed to relax, while the bottom ½ layers are fixed.

The Mo-terminated $Mo_2C(001)$ and C-terminated $Mo_2C(001)$ surfaces, denoted as Mo-$Mo_2C(001)$ and C-$Mo_2C(001)$, respectively, were modeled by periodic four-layer Mo_2C slabs using the optimized lattice constants of a = 4.767 Å, b = 6.060 Å, and c = 5.242 Å. These values closely match the experimental results of a = 4.724 Å, b = 6.004 Å, and c = 5.199 Å for orthorhombic Mo_2C.[37] The periodically repeated unit cells were separated by 20.0 Å of vacuum in the z-direction. A (1 x 1) unit cell was used for calculations to determine oxygen adsorption energy versus coverage. The reported differential binding energy for oxygen at varying coverages was calculated relative to H_2 and H_2O in the gas phase (eq 9):

$$BE = E_{nO/Mo-Mo_2C} + E_{H_{2(gas)}} - E_{(n-1)O/Mo-Mo_2C} - E_{H_2O_{(gas)}} \quad (9)$$

where $E_{nO/Mo-Mo_2C}$ is the energy of the Mo-terminated surface with *n* oxygen atoms adsorbed, $E_{(n-1)O/Mo-Mo_2C}$ is the energy of the Mo-terminated surface with *n-1* oxygen atoms adsorbed,

Pursuant to the DOE Public Access Plan, this document represents the authors' peer-reviewed, accepted manuscript. The published version of the article is available from the relevant publisher.

$E_{H_2(gas)}$ is the energy of gas phase H_2 and $E_{H_2O(gas)}$ is the energy of gas phase H_2O. The differential binding energies of oxygen on the C-terminated surface were calculated analogously. For the Mo-Mo_2C(001) and C-Mo_2C(001) surfaces, 1 monolayer (ML) of O was defined as a surface with an O/Mo ratio of 1:1 and an O/C ratio of 2:1, respectively. To determine the relevant surface coverage of oxygen under reaction conditions, we constructed the phase diagram for O/Mo-Mo_2C(001) and O/C-Mo_2C(001) by calculating the grand potential (Ω) at discrete coverages of 0.25 ML, 0.50 ML, 0.75 ML, 1.00 ML and 1.25 ML.[38,39] The grand potential for oxygen coverage on the Mo-Mo_2C(001) system is defined as eq 10:

$$\Omega = E_{nO/Mo-Mo_2C} - E_{Mo-Mo_2C} + N_{H_2} * \mu_{H_2} - N_{H_2O} * \mu_{H_2O} - T * S \quad (10)$$

where $E_{Mo\text{-}Mo2C}$ is the total energy of the clean Mo-Mo_2C(001) slab, μ_i is the chemical potential of species *i*, *T* is the absolute temperature, and *S* is the entropy of the O/Mo-Mo_2C(001) system. The chemical potential of species *i* was calculated by eq 11:

$$\mu_i = k_B * T * ln\frac{P_i}{P^o} + E_i - T * S_i \quad (11)$$

where k_B is the Boltzmann constant, P_i is the partial pressure of speices *i*, P^o is the reference pressure of 1 atm, E_i is the total energy of species *i* in the gas phase, and S_i is the entropy of gas phase species *i*. The phase diagram for O/C-Mo_2C(001) was calculated analogously.

Subsequent calculations of adsorption energies of reaction intermediates and identification of minimum energy pathways required (2 x 2) unit cells due to the size of the intermediates studied. Minimum energy pathways and transition state energies for elementary steps were located using the climbing image nudged elastic band (CI-NEB) method.[40] At least seven intermediate images were interpolated between the reactant and product states. The transition state was confirmed by

Pursuant to the DOE Public Access Plan, this document represents the authors' peer-reviewed, accepted manuscript. The published version of the article is available from the relevant publisher.

vibrational frequency calculations yielding a single imaginary frequency along the reaction coordinate.

3. RESULTS AND DISCUSSION

3.1. Catalyst Characterization

The as-prepared carbide material exhibited XRD peaks characteristic of orthorhombic β-Mo_2C (Figure 1a). The broad diffraction peaks are indicative of a nano-crystalline material, and line broadening analysis indicates a crystallite size of 10 nm. Similar to Mo_2C materials prepared previously by similar methods, the BET surface area was 69 m^2/g.[20,22] The catalyst exhibited a H-adsorption site density, determined by H_2 chemisorption, of 54 μmol/g, which corresponds to ca. 5% surface coverage (assuming a total site density of 1×10^{19} sites/m^2).[41]

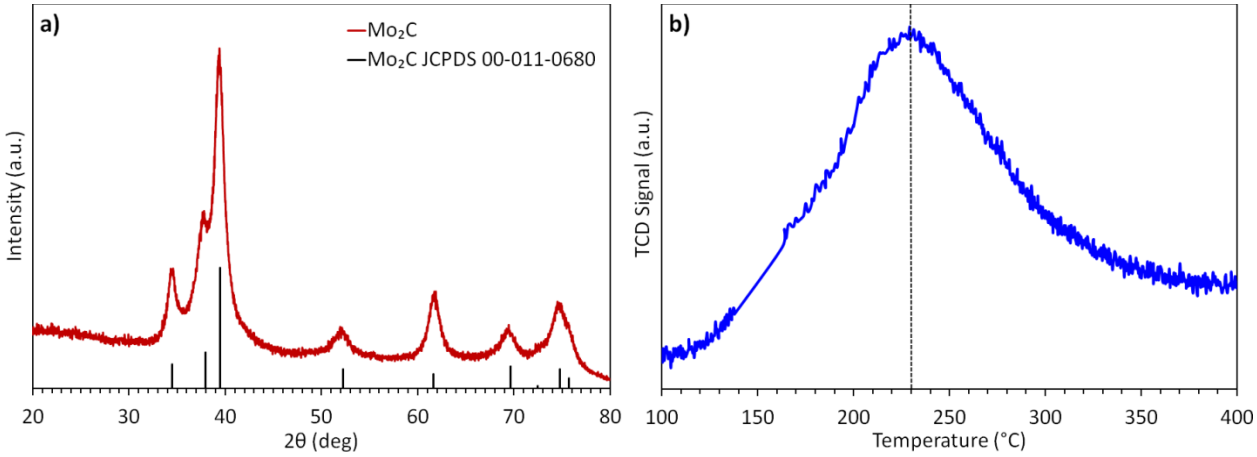

Figure 1. Mo_2C characterization: (a) XRD pattern including reference and (b) NH_3-TPD spectrum.

Total acid site density, as determined by NH_3-TPD, was 441 μmol/g and the TPD profile is shown in Figure 1b. The Mo_2C catalyst exhibited a broad desorption peak centered at ca. 230 °C, similar to that observed by Bej et al.[6] This result indicates that the Mo_2C catalyst possesses sites that are weakly acidic in nature; these sites may be attributed to surface hydroxyls due to incomplete removal of oxygen during the H_2 pretreatment.[9,42] Sullivan et al.[9] demonstrated that

Pursuant to the DOE Public Access Plan, this document represents the authors' peer-reviewed, accepted manuscript. The published version of the article is available from the relevant publisher.

Brønsted acid sites are formed on the Mo_2C surface in the presence of oxygen co-feed, and Hibbitts et al.[42] computationally showed that surface hydroxyls present on the surface of oxidized oxophilic MO_x species exhibit acidic character. The density of these acidic sites on Mo_2C is equivalent to ca. 38% surface coverage (assuming a total site density of 1×10^{19} sites/m^2).[41] Based on H_2 chemisorption and NH_3-TPD, the surface of Mo_2C has ca. 8 times more acidic sites than metallic-like H-adsorption sites following pretreatment in H_2 at 400 °C.

3.2. Temperature Programmed Reaction

3.2.1. Acetic Acid

TPRxn with acetic acid and H_2 was performed to evaluate the deoxygenation performance of Mo_2C, and the results are provided in Figure 2 and Table 1. Acetic acid conversion started at ca. 250 °C and reached greater than 90% by 600 °C (Figure 2a). It should be noted that these TPRxn experiments do not measure steady-state rates, thus, reaction rates and product selectivities include the effects of deactivation/catalyst stabilization. The conversion of acetic acid coincided with the consumption of H_2 (Figure 2a and Table 1), with a maximum rate of H_2 consumption observed at ca. 425 °C. This temperature is in good agreement with the observed temperature at which Mo_2C exhibited its maximum rate of H_2O production (Figure 2b).

Pursuant to the DOE Public Access Plan, this document represents the authors' peer-reviewed, accepted manuscript. The published version of the article is available from the relevant publisher.

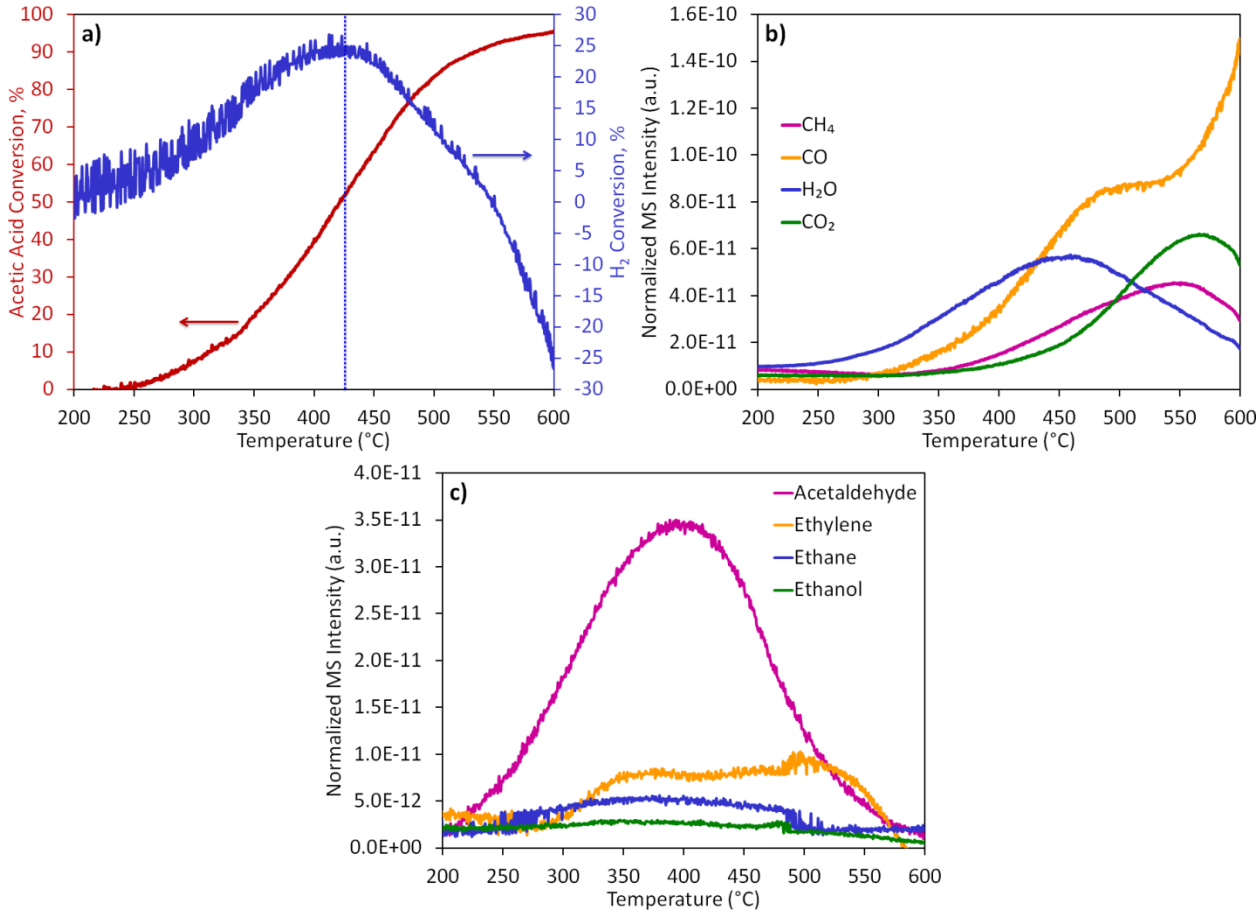

Figure 2. Conversion of (a) acetic acid and hydrogen and production of (b) CH_4, CO, H_2O, and CO_2 and (c) hydrodeoxygenation products (acetaldehyde, ethanol, ethylene, and ethane) over Mo_2C during acetic acid TPRxn experiments. Positive values of H_2 conversion correspond to H_2 consumption while negative values correspond to H_2 evolution.

Pursuant to the DOE Public Access Plan, this document represents the authors' peer-reviewed, accepted manuscript. The published version of the article is available from the relevant publisher.

Table 1. Reaction rates and H_2/oxygenate molar consumption ratios for Mo_2C during TPRxn experiments with acetic acid, ethanol, and acetaldehyde.

Oxygenate Reactant	Temperature (°C)	Oxygenate Conversion (%)	Oxygenate Consumption Rate Normalized by H-Adsorption Sites ($mol_{Ox}\ mol_{H\text{-}sites}^{-1}\ s^{-1}$)	Oxygenate Consumption Rate Normalized by NH_3-Adsorption Sites ($mol_{Ox}\ mol_{NH_3\text{-}sites}^{-1}\ s^{-1}$)	H_2/oxygenate Molar Consumption Ratio[a]
Acetic Acid	350	19.4	0.035	0.004	3.5
	300	7.7	0.014	0.002	3.6
	250[b]	--	--	--	--
Ethanol	350	77.4	0.53	0.06	-0.16
	300	50.0	0.34	0.04	-0.27
	250	21.1	0.14	0.017	-0.28
Acetaldehyde	350	44.3	0.11	0.014	1.0
	300	25.5	0.06	0.008	1.4
	250	11.1	0.03	0.003	2.3

[a]A positive value implies that acetic acid conversion involves H_2 incorporation while a negative value indicates the evolution of H_2. [b]Conversion of acetic acid at 250°C was too low to measure.

H_2 consumption (and evolution) corresponded to multiple reaction pathways that varied with temperature. From 250 – 400 °C, Mo_2C favored hydrogenation-dehydration pathways (eqs 6–8, C-O cleavage), producing primarily acetaldehyde and ethylene (Figure 2c). Negligible amounts of ethanol were observed and ethylene was not readily hydrogenated to ethane. This result is similar to that reported by Ren et al. for the conversion of C_3 oxygenates over WC, in which they observed the formation of predominantly propylene.[12] The lack of significant amounts of ethanol and ethane in the product stream from Mo_2C suggests that consumed H_2 was used preferentially to form H_2O (potentially by the removal of surface hydroxyls to regenerate the deoxygenation active site), instead of hydrogenating acetaldehyde (to ethanol) and ethylene (to ethane) at hydrogenation sites. In contrast, it has been reported that the dominant acetic acid reaction pathway over supported Pt catalysts under similar conditions was decarbonylation (eq 2, C-C cleavage).[43] Based on the observed selectivity towards C-O cleavage below 400 °C over Mo_2C, the remainder of this paper will focus primarily on this deoxygenation chemistry, and TPRxn

Pursuant to the DOE Public Access Plan, this document represents the authors' peer-reviewed, accepted manuscript. The published version of the article is available from the relevant publisher.

experiments with ethanol and acetaldehyde as the feed were performed to further probe these hydrogenation-dehydration pathways (Sections 3.2.2 and 3.2.3).

Over the temperature range of 400 – 550 °C, Mo_2C shifted from C-O cleavage reactions to C-C cleavage reactions, producing primarily CH_4, CO, and CO_2 (Figure 2b) through decarbonylation (eq 2) and decarboxylation (eq 3), likely coupled with water gas shift (WGS) and methane steam reforming (MSR). Mo_2C has been reported to be an active catalyst for WGS and MSR.[20-22,44,45] Above 550 °C, the dominant pathway over Mo_2C was gasification (eq 1), as indicated by the evolution of H_2 (Figure 2a) and increased production of CO (Figure 2b).

3.2.2. Ethanol

Due to the lack of ethanol observed during the conversion of acetic acid, we performed TPRxn experiments with ethanol as the feed to probe its role as an intermediate (Figure 3). The Mo_2C catalyst was active for ethanol conversion at 150 °C and favored the dehydration of ethanol to form ethylene and H_2O (although some CO and CH_4 production was observed at temperatures greater than 400 °C). Normalized by either H-adsorption sites or NH_3-adsorption sites, the rate of ethanol consumption (i.e., dehydration) was an order of magnitude higher than the rate of acetic acid consumption (Table 1). At 300 °C, the rate of ethanol consumption over Mo_2C was 0.04 $mol_{ethanol}$ $mol_{NH_3\text{-}sites}^{-1}$ s^{-1}, compared to a reported value for HZSM-5, a zeolite catalyst known to possess strong Brønsted acidic sites, of 0.726 $mol_{ethanol}$ $mol_{NH_3\text{-}sites}^{-1}$ s^{-1}.[46]

Although H_2 was co-fed with ethanol, H_2 production was observed over Mo_2C at temperatures below ca. 375 °C (Figure 3a and Table 1). Interestingly, H_2 was produced prior to ethylene being observed in the product stream, suggesting that cleavage of the O-H bond in ethanol upon adsorption to the Mo_2C surface and formation of an ethoxy intermediate is the first

Pursuant to the DOE Public Access Plan, this document represents the authors' peer-reviewed, accepted manuscript. The published version of the article is available from the relevant publisher.

step in the dehydration reaction. This result is consistent with the work of Ren et al., which computationally showed that the first step in propanol adsorption to WC was O-H bond scission.[12] H_2 consumption increased with increasing temperature, with a maximum at ca. 420 °C (Figure 3a). This temperature coincides with the maximum rate of H_2O production (Figure 3b), indicating that elevated temperature was required to remove oxygen from the Mo_2C surface as H_2O. Above 450 °C, H_2, CH_4, and CO are produced (Figure 3b), indicating that the favored pathway over Mo_2C shifted to ethanol decomposition. These ethanol TPRxn results suggest that, at temperatures below 400 °C, ethanol dehydration is not likely the rate limiting step in the conversion of acetic acid to ethylene (assuming a pathway that proceeds through an ethoxy intermediate), as ethanol will most likely be consumed as quickly as it is produced from acetaldehyde.

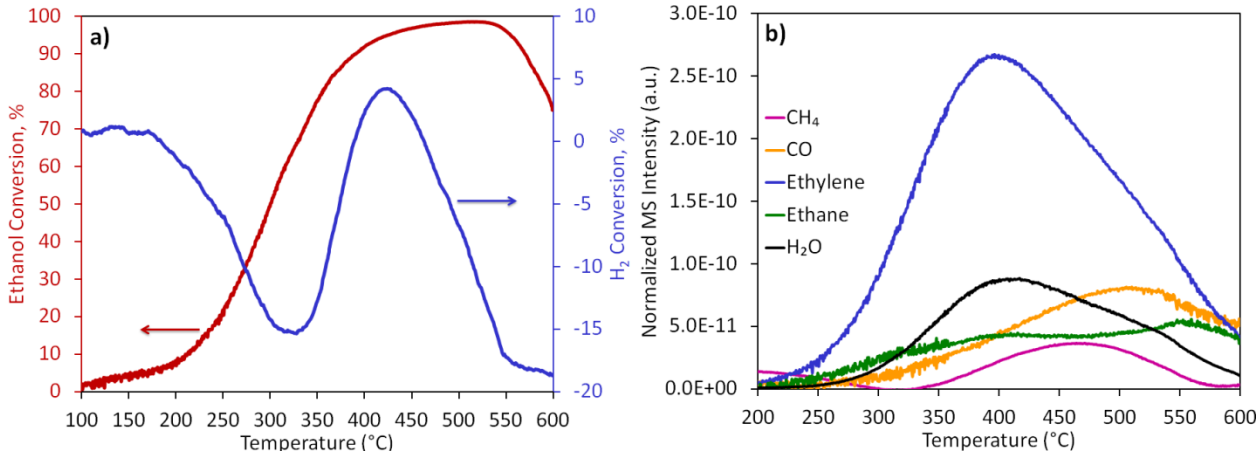

Figure 3. Conversion of (a) ethanol and hydrogen and production of (b) CH_4, CO, ethylene, ethane, and H_2O over Mo_2C during ethanol TPRxn experiments. Positive values of H_2 conversion correspond to H_2 consumption while negative values correspond to H_2 evolution.

3.2.3. Acetaldehyde

The conversion of acetaldehyde, the dominant hydrogenation-dehydration product from acetic acid observed over Mo_2C, was also investigated using TPRxn, and the results are shown in Figure 4. Similar to acetic acid, H_2 consumption coincided with acetaldehyde conversion (Figure

Pursuant to the DOE Public Access Plan, this document represents the authors' peer-reviewed, accepted manuscript. The published version of the article is available from the relevant publisher.

4a), giving a H_2/acetaldehyde molar consumption ratio of ca. 1 at 300–350 °C (Table 1). This ratio is consistent with the formation of ethanol and/or ethylene. The product distribution over Mo_2C varied considerably with temperature (Figure 4b). Below 300 °C, the dominant product was ethanol, formed by the hydrogenation of acetaldehyde. Since limited hydrogenation was observed during acetic acid TPRxn experiments, this observed enhancement in hydrogenation may be due to the lower temperature or a stabilization period for the Mo_2C catalyst. For the hydrodeoxygenation of anisole, Lee et al. demonstrated enhanced hydrogenation activity (i.e., formation of cyclohexane instead of benzene) over Mo_2C during the initial period of time on stream (TOS), and attributed this stabilization to the *in-situ* oxidation of the carbide surface.[18] It should also be noted that the thermodynamic equilibrium between ethanol and acetaldehyde + H_2 favors ethanol below ca. 330 °C and acetaldehyde + H_2 above ca. 330 °C.[47] However, at 300 °C over the Mo_2C catalyst, the approach to equilibrium for hydrogenation of acetaldehyde to produce ethanol (and subsequently ethylene) was 0.012, indicating that hydrogenation was not thermodynamically limited under these conditions. As temperature increased above 300 °C, ethanol production decreased with a concomitant increase in ethylene and H_2O production. As observed previously, a minimal amount of ethane was observed. At temperatures above 450 °C, the dominant product over the Mo_2C catalyst was CO (Figure 4b). The relative observed extents of hydrogenation and dehydration are consistent with the ratio of metallic-like H-adsorption sites to acidic sites on the Mo_2C surface. Overall, results from these TPRxn experiments over Mo_2C with acetic acid, ethanol, and acetaldehyde, at temperatures between 300–400 °C (conditions relevant to *ex-situ* CFP), suggest that (1) C-O bond cleavage is preferred over C-C bond cleavage and (2) hydrogenation of surface-bound intermediates proceeds slower than C-O bond cleavage,

Pursuant to the DOE Public Access Plan, this document represents the authors' peer-reviewed, accepted manuscript. The published version of the article is available from the relevant publisher.

which may be a result of the low concentration of sites capable of activating H_2 (ca. 5% of the surface of Mo_2C based on H_2 chemisorption).

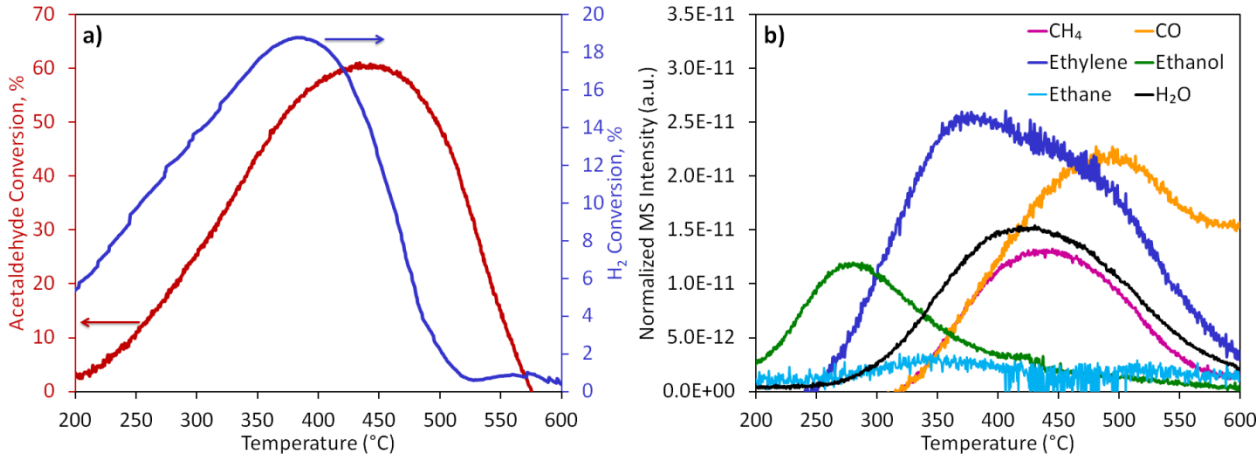

Figure 4. Conversion of (a) acetaldehyde and hydrogen and production of (b) CH_4, CO, ethylene, ethanol, ethane, and H_2O over Mo_2C during acetaldehyde TPRxn experiments.

3.3. *In-situ* DRIFTS

3.3.1. Hydrogen Reduction

Figure 5 displays DRIFTS spectra for Mo_2C samples after first reducing in flowing H_2 (purple trace), and then reducing in flowing D_2 (red trace). For the hydrogen-reduced sample, prominent peaks in the range of 2900 to 3200 cm^{-1} and a sharp peak at 1406 cm^{-1} are consistent with the stretching and bending modes of C-H bonds, respectively, and suggest that the high temperature H_2 reduction forms C-H bonds on the Mo_2C surface. Deuterium reduction (of the previously H_2-reduced sample) produced negative peaks in the 2900 – 3200 cm^{-1} range and at 1406 cm^{-1} and positive peaks in the range of 2200 – 2500 cm^{-1} and 995 cm^{-1}. Each cluster of positive peaks is red-shifted with respect to the corresponding negative peaks by an energy expected from isotopic substitution (ca. $\sqrt{1/2}$), indicating that C-D peaks have replaced C-H peaks. No obvious peaks corresponding to Mo-H bonds are seen following high-temperature H_2

Pursuant to the DOE Public Access Plan, this document represents the authors' peer-reviewed, accepted manuscript. The published version of the article is available from the relevant publisher.

reduction. The stretching frequency of Mo-H bonds has been reported to be in the range of ca. 1730 cm^{-1} for gas-phase MoH_x species.[48] These results suggest that the metallic-like H-adsorption sites probed by H_2 chemisorption in Section 3.1 may be attributed, at least partially, to carbidic carbon atoms present on the Mo_2C surface.

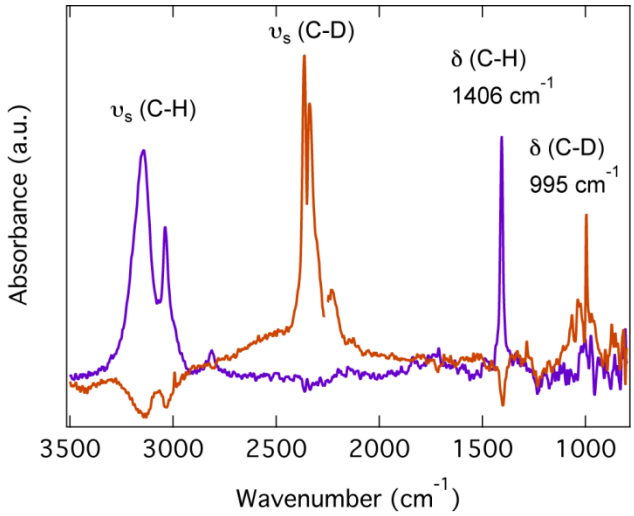

Figure 5. Room-temperature DRIFTS spectra of a Mo_2C sample following reduction at 400 °C. Sample was first reduced in H_2 (purple trace), followed by a reduction in D_2 (red trace).

3.3.2. Acetic Acid Adsorption

Figure 6a displays DRIFTS spectra for a H_2-reduced Mo_2C sample exposed to acetic acid for either a short (early exposure) or long (saturation exposure) amount of time. The dominant peaks for saturation exposure are the expected vibrational modes for *gas-phase* acetic acid, in addition to peaks i – vii that correspond to the vibrational modes of *chemisorbed* acetic acid molecules. At early times, two main peaks in the C=O stretching region at 1800 cm^{-1} and 1782 cm^{-1} and a shoulder at ca. 1716 cm^{-1} (peaks i – iii) were observed. There were also three peaks in the C-O stretching region between 1100 and 1400 cm^{-1} (peaks iv – vi) and a peak around 1000 cm^{-1}, a region consistent with Mo-O bonds. When the acetic acid saturated sample was evacuated, the adsorbed acetic acid peaks evolved with time (Figure 6b). Peaks i and ii (1800 and 1782 cm^{-1})

Pursuant to the DOE Public Access Plan, this document represents the authors' peer-reviewed, accepted manuscript. The published version of the article is available from the relevant publisher.

diminished significantly with time, leaving a dominant peak at 1714 cm^{-1} (iii) and a smaller peak at 1760 cm^{-1} (viii) after overnight evacuation.

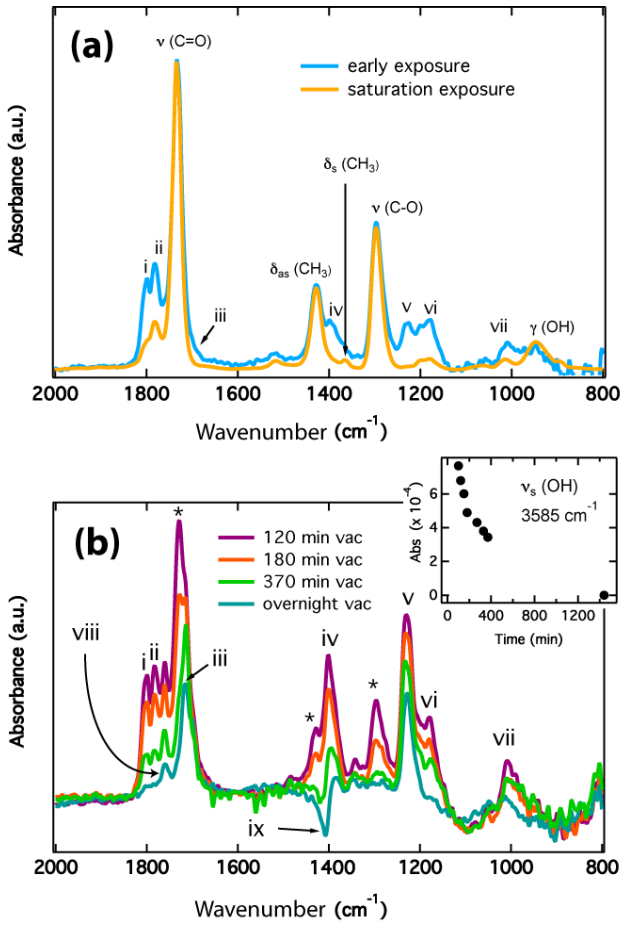

Figure 6. (a) DRIFTS spectra for Mo_2C sample exposed to low coverage of acetic acid (early exposure) and saturation coverage (saturation exposure). Peaks for free acetic acid molecules are labeled with their corresponding vibrational modes, while peaks for adsorbed molecules are labeled i – vii. (b) Series of DRIFTS spectra for a Mo_2C sample saturated with acetic acid (e.g., saturation exposure from panel a), and then evacuated (ca. 0.5 Torr) continuously for the time denoted in the legend. Peaks i – viii denote vibrational modes of adsorbed species, whereas asterisks denote vibrational modes of gas-phase (or potentially physisorbed) acetic acid molecules.

The region from ca. 1200 cm^{-1} to 1410 cm^{-1} encompasses both C-O (C-OH) stretching and C-H bending/deformation. After overnight evacuation, a strong peak at 1230 cm^{-1} (v) dominated this region. Additionally, a positive shoulder around 1380 cm^{-1} (iv) accompanied a prominent negative peak at 1406 cm^{-1} (ix). The 1380 cm^{-1} and 1230 cm^{-1} peaks (iv and v) are in the same

Pursuant to the DOE Public Access Plan, this document represents the authors' peer-reviewed, accepted manuscript. The published version of the article is available from the relevant publisher.

range as peaks assigned by Flaherty et al. to bidentate and monodentate formate (1360 and 1267 cm^{-1}), respectively.[49] The 1406 cm^{-1} peak matches the C-H bending mode observed for the H_2-reduced sample, indicating the eventual *desorption* of some fraction of the C-H bonds formed in the reduction step, either through the adsorption of acetic acid or *via* dynamic evacuation (or both). A small peak at ca. 1346 cm^{-1} (unlabeled) is consistent with C-H deformations in the bound acetic acid molecules. Interestingly, peak v at 1230 cm^{-1} had a shoulder at 1178 cm^{-1} (peak vi, prominent in early exposure, Figure 6a), and the intensity of peak vi systematically decreased with time under dynamic vacuum (Figure 6b). Since this region is consistent with ν(C-O) of monodentate acetic acid, we hypothesize that peaks v and vi may arise from two different species of the monodentate adsorbate: the deprotonated acetate adsorbate (v) and the protonated acid adsorbate (vi). In this case, the slow disappearance of peak vi could represent a slow deprotonation step, for example, H atom transfer to surface Mo or C atoms. Interestingly, the inset of Figure 6b demonstrates that the characteristic O-H stretching mode, ν(OH), of the adsorbed acetic acid molecules also decreased slowly with time and was completely absent after overnight evacuation. This observation supports our assignment of peaks v and vi as the adsorbed monodentate acetate and acid, respectively. These observations are consistent with the results from ethanol TPRxn over Mo_2C, in which the stronger O-H bond in ethanol was cleaved upon adsorption to the carbide surface.

Two regions enable tentative conclusions to be drawn regarding Mo-O and Mo-H bonding. The low-energy range (below 1200 cm^{-1}) was dominated by a broad peak centered around 1000 cm^{-1} (peak vii), a range typically attributed to Mo-O and Mo=O stretching frequencies.[50] Peak vii (1760 cm^{-1}) was relatively strong after overnight evacuation. This peak position is near the strong 1730 cm^{-1} peak assigned to Mo-H stretching in gas-phase MoH_x mixtures.[48] However,

Pursuant to the DOE Public Access Plan, this document represents the authors' peer-reviewed, accepted manuscript. The published version of the article is available from the relevant publisher.

other studies have assigned peaks at significantly lower energies (e.g., 980 – 1260 cm^{-1}) to Mo-H stretching.[49,51] Thus, we leave it as an open possibility that H atoms from some acetic acid molecules bind to Mo surface atoms (peak vii) in addition to C surface atoms (peak x, *vide infra*).

3.3.2.1.Isotope Substitution

Isotope experiments enable us to conclusively assign each of the peaks observed above and develop a comprehensive picture of how acetic acid adsorbs (and reacts) on the Mo_2C surface. We explored four Mo_2C samples subjected to different treatments: (1) H_2 reduction, followed by acetic acid adsorption (denoted as AA), (2) H_2 reduction followed by deuterated acetic acid (CH_3COOD, denoted as AA-d) adsorption, (3) H_2 reduction followed by 1-^{13}C acetic acid ($CH_3{}^{13}COOH$, denoted as AA-13C) adsorption, and (4) D_2 reduction followed by acetic acid adsorption. Figure 7 summarizes the pertinent DRIFTS spectra for isotopic substitution experiments, and peak positions are tabulated in Table 2.

Pursuant to the DOE Public Access Plan, this document represents the authors' peer-reviewed, accepted manuscript. The published version of the article is available from the relevant publisher.

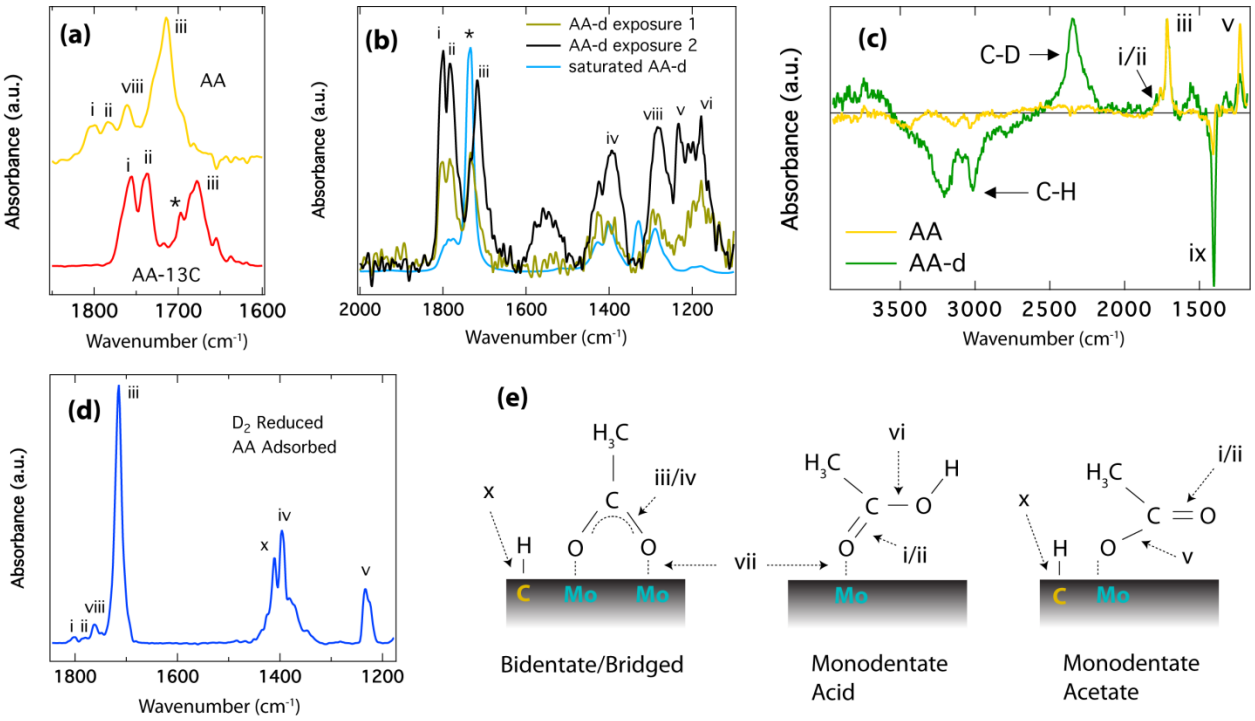

Figure 7. (a) DRIFTS spectra in C=O stretching region for H_2-reduced Mo_2C samples exposed to AA and AA-13C and then evacuated for varying amounts of time. Gas-phase acetic acid peaks are denoted with asterisks. (b) H_2-reduced Mo_2C sample exposed to low AA-d pressures to arrive at sub-monolayer coverages. The blue spectrum shows the same sample after saturation exposure for comparison. (c) Comparison of DRIFTS spectra for H_2-reduced Mo_2C samples that are treated with either AA or AA-d and evacuated overnight. (d) DRIFTS spectrum for D_2-reduced Mo_2C sample exposed to AA and then evacuated overnight. (e) Schematics of the three different acetic acid adsorbates deduced from DRIFTS spectra. Primary peaks are labeled i – x.

Table 2. Peak positions for isotopic substitution DRIFTS experiments.

Peak	AA (cm^{-1})	AA-d (cm^{-1})	AA-13C (cm^{-1})	Assignment
i	1800	1791	1756	ν(C=O) monodentate acetate/acid
ii	1782	1782	1738	ν(C=O) monodentate acetate/acid
iii	1716	1716	1677	ν_s(C-O) bidentate acetate
iv	1386	1386	1334	ν_{as}(C-O) bidentate acetate
v	1230	1230	1174	ν(C-O) monodentate acetate
vi	1178	1178	1166	ν(C-O) monodentate acid
vii	1008	-	-	ν(Mo-O)
viii	1760	1290	-	ν(Mo-H)
ix	1406 (negative)	1406	1406	δ(C-H) (from H_2 reduction)
x	1406 (positive)	Not performed	Not performed	δ(C-H) (dissociated from acetic acid, requires D_2 reduction)

Pursuant to the DOE Public Access Plan, this document represents the authors' peer-reviewed, accepted manuscript. The published version of the article is available from the relevant publisher.

Figure 7a compares the C=O stretching region for H_2-reduced Mo_2C treated with AA and AA-13C, and subsequently evacuated. Peaks i, ii, and iii all red-shift considerably for AA-13C adsorption relative to AA adsorption, confirming the relation of these peaks to the carboxylate carbon. The energetic shift of peaks i – iii, relative to gas-phase acetic acid, provide some insight into their assignments. The red-shift of peak iii, relative to gas-phase acetic acid, is consistent with a lengthening of the C=O bond upon adsorption. Such lengthening is assigned to bidentate acetate adsorption, where the bond order of each C-O bond is between 1 and 2, and accordingly has lengths between single- and double bonds. In contrast, peaks i and ii are both blue-shifted relative to gas-phase acetic acid, suggesting that the C=O double bond of *monodentate* adsorbates are slightly shortened relative to the unbound molecule.

Figure 7b shows the spectrum for a Mo_2C sample that was first reduced with H_2, and then treated with AA-d for short exposure times, in order to achieve sub-monolayer coverage. For the first exposure, the only adsorbate peaks were i, ii, and vi, all of which have been assigned to monodentate acetic acid. The initial presence of peak vi suggests that the dominant species at these low initial coverages is the *monodentate* acid species. As the sample was exposed for a longer time (exposure 2), peaks iii, iv, and v appeared. From Table 2, the delayed observation of these peaks is consistent with the bidentate and deprotonated acetate adsorbates arising *via* a kinetically limited conversion of the monodentate acetate adsorbate.

Clearly, the formation of the monodentate and bidentate acetate adsorbates suggests that the acidic H atom is stripped from some acetic acid molecules upon adsorption, and is likely transferred to surface C and/or Mo atoms. As discussed above, peak viii was observed at 1760 cm^{-1} for AA-treated Mo_2C, and was tentatively assigned to Mo-H bonds formed *via* H transfer from the adsorbed acetic acid molecule. If this assignment were correct, one would expect this

Pursuant to the DOE Public Access Plan, this document represents the authors' peer-reviewed, accepted manuscript. The published version of the article is available from the relevant publisher.

peak to shift to ca. 1290 cm^{-1} for a Mo-D bond formed by AA-d adsorption. Interestingly, no peak was observed at 1760 cm^{-1} for the AA-d treated sample, but a rather strong peak at 1290 cm^{-1} (viii) was observed for the AA-d treated sample in Figure 7b (exposure 2). Thus, these data are consistent with some fraction of Mo-H bonds formed on the Mo_2C surface by H transfer from adsorbed acetic acid molecules. Unfortunately, AA-13C adsorption produces a peak at 1756 cm^{-1} (Figure 7a, peak i) for the monodentate C=O stretch, potentially masking the 1760 cm^{-1} peak that would be observed for Mo-H bonds on this sample. If the 1760 cm^{-1} peak observed for AA-treated Mo_2C is in fact due to Mo-H bonds, the absence of this peak for H_2-reduced Mo_2C suggests that these Mo-H bonds are not formed at high temperatures in the presence of H_2.

Two separate isotope experiments confirm that H atoms are transferred from adsorbed acetic acid molecules to *carbon atoms* on the Mo_2C surface. Figure 7c compares the spectra of two H_2-reduced Mo_2C samples that were exposed to either AA or AA-d and then evacuated overnight. The AA-d treated sample spectrum exhibits more intense negative peaks for C-H stretching (labeled C-H) and bending (peak ix), than that of the AA-treated sample, in addition to a broad envelope of positive peaks between 2100 and 2500 cm^{-1} that is absent for the AA-treated sample. These observations indicate that D atoms from some fraction of adsorbed AA-d molecules transfer to C atoms on the Mo_2C surface. Figure 7d shows the spectrum for a Mo_2C sample that was first reduced with D_2, and then treated with acetic acid. Peaks i, ii, iii, v, and viii were all observed in the same positions as for the H_2-reduced, AA-treated sample. Importantly, D_2 reduction moved peak ix (1406 cm^{-1}, negative), corresponding to C-H bonds formed in the reduction step, below 1000 cm^{-1}. This shift allows two important new peaks to be observed following acetic acid adsorption at 1406 cm^{-1} (peak x) and 1386 cm^{-1} (peak iv). Peak x (1406 cm^{-1}, positive) is consistent with the formation of new C-H bonds upon acetic acid adsorption. Since

Pursuant to the DOE Public Access Plan, this document represents the authors' peer-reviewed, accepted manuscript. The published version of the article is available from the relevant publisher.

the sample was reduced with D_2 and should have C-D bonds following reduction, this suggests that the acidic protons of some acetic acid molecules dissociate and bind to C atoms on the Mo_2C surface during adsorption, consistent with our proposal of mixed bidentate and monodentate acetate adsorption. Additionally, peak iv (1386 cm^{-1}) was observed clearly for the D_2-reduced sample, whereas the negative 1406 cm^{-1} peak (peak viii, desorbed C-H) obscured this peak for the H_2-reduced AA-treated sample, where it can only be observed as a weak shoulder after appreciable evacuation.

3.3.2.2.Acetic Acid Adsorption Geometries

Figures 6 and 7 provide a complete picture of the adsorption mechanism and geometries of acetic acid on the Mo_2C material. Schematics of the adsorption geometries are summarized in Figure 7e, with peak assignments of the main observed vibrational modes.

3.3.3. Acetic Acid Reaction

Using the peak assignments and adsorption geometries determined above, temperature-dependent DRIFTS measurements were employed to follow the reaction of acetic acid on the surface of the Mo_2C particles. Figure S2 shows detailed temperature-dependent spectra for multiple samples, and Figure 8 summarizes the evolution of several surface species, as derived from Figure S2. In these temperature-dependent DRIFTS spectra (Figure S2), negative peaks correspond to desorption of a particular adsorbate *or* its conversion to another adsorbate (e.g., bidentate to monodentate acetate). Positive peaks correspond to the creation of a new chemisorbed or physisorbed adsorbate.

Figure 8 displays temperature profiles for several peaks in a variety of conditions, in order to correlate the appearance and disappearance of surface adsorbates and reaction products. Figure 8a shows that when the Mo_2C sample (diluted in KBr) was heated under vacuum, the bidentate

Pursuant to the DOE Public Access Plan, this document represents the authors' peer-reviewed, accepted manuscript. The published version of the article is available from the relevant publisher.

adsorbate is steadily depleted up to ca. 250 – 270 °C, at which point it is fully depleted. This depletion of the bidentate adsorbate was accompanied by an increase in the peak intensities for the monodentate species, suggesting interconversion from bidentate to monodentate acetate. Peak intensities for the monodentate adsorbates continue to rise until ca. 270 °C, at which point the monodentate form begins to rapidly deplete. This rapid depletion most likely results from the fact that fresh monodentate adsorbate is no longer being provided by the conversion of bidentate and additional reactions occurring at these high temperatures also contribute to this rapid depletion (*vide infra*).

Figure 8b shows that when a similar Mo_2C sample is heated in a flow of 4% hydrogen, the monodentate adsorbate begins to be abruptly depleted above ca. 95 °C. Importantly, this depletion is not observed for the sample that is degassed in vacuum, suggesting that a consistent supply of hydrogen atoms from the Mo_2C surface is necessary to efficiently drive this particular reaction step. It is interesting to contrast the qualitatively similar behavior of the bidentate adsorbate in Figures 8a and 8b with the significantly earlier onset for depletion of the monodentate form when H_2 is continually supplied to the Mo_2C surface. This stark difference suggests that the monodentate adsorbate(s) are primarily responsible for the majority of high-temperature products.

Figure 8c displays DRIFTS temperature profiles for an undiluted Mo_2C sample that was supplied with a constant overpressure of acetic acid while it was heated in flowing 4% hydrogen. This experiment enables the easy observation of *gas-phase products* in addition to adsorbates. An abrupt depletion of the monodentate adsorbates occurs above ca. 140 °C and the slope of the temperature profile changes above ca. 250 °C (more rapid depletion above 250 °C). The concomitant rapid increase of peaks corresponding to CO and CO_2 above ca. 250 °C suggest that

Pursuant to the DOE Public Access Plan, this document represents the authors' peer-reviewed, accepted manuscript. The published version of the article is available from the relevant publisher.

this second onset of depletion corresponds (at least in part) to direct decarbonylation and decarboxylation. The first depletion, beginning between ca. 100 and 150 °C may be correlated to the rise of ethylene (C_2H_4) peaks above ca. 200 °C. These results are in good agreement with the acetic acid TPRxn experiments over Mo_2C, as production of acetaldehyde and ethylene occurred at lower temperatures (200-400 °C), while the production of CO and CO_2 did not begin to dominate until temperatures above 400 °C.

Pursuant to the DOE Public Access Plan, this document represents the authors' peer-reviewed, accepted manuscript. The published version of the article is available from the relevant publisher.

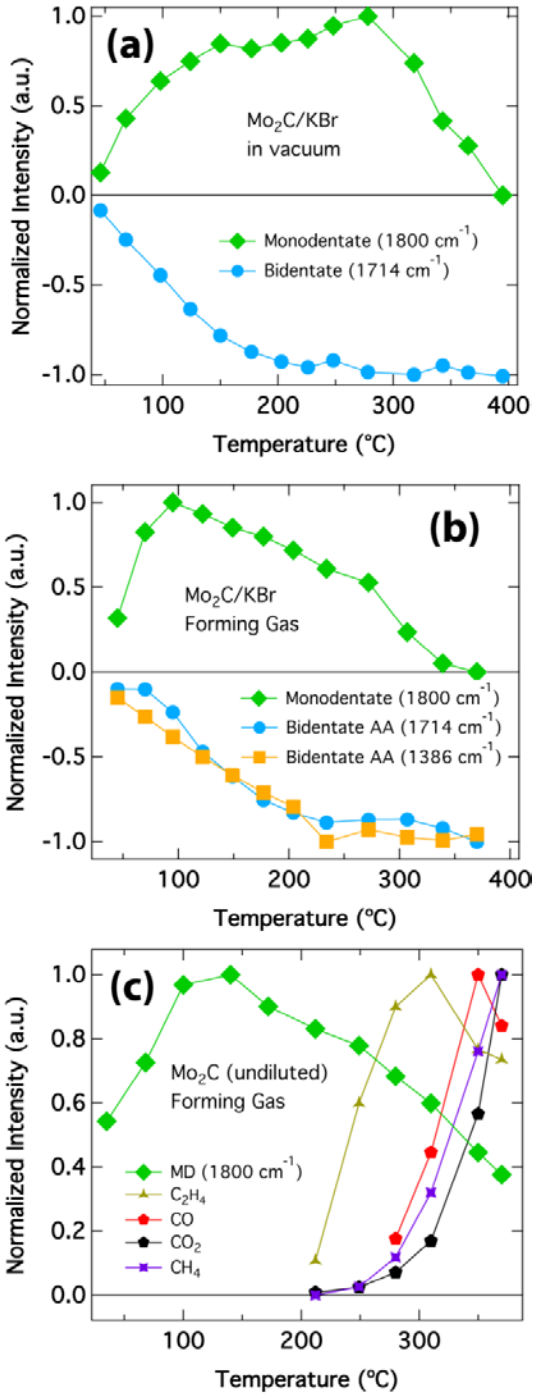

Figure 8. Temperature profiles for adsorbates and reaction products observed in temperature-dependent DRIFTS experiments. All samples were first exposed to acetic acid for several minutes. (a) KBr-diluted Mo_2C sample. After acetic acid exposure, gas-phase acetic acid was removed by evacuation for several hours, and the sample was then heated in vacuum. (b) KBr-diluted Mo_2C sample. After acetic acid exposure, gas-phase acetic acid was removed by evacuation for several hours and the sample was then heated in flowing 4% H_2 in Ar. (c) Undiluted Mo_2C sample heated in flowing 4% H_2 in Ar, and with a constant overpressure of acetic acid.

Pursuant to the DOE Public Access Plan, this document represents the authors' peer-reviewed, accepted manuscript. The published version of the article is available from the relevant publisher.

3.4. X-ray Photoelectron Spectroscopy

XPS was used to probe the surface chemistry of Mo_2C after various treatments without exposure to air, and provide guidance on the surface termination for the Mo_2C DFT model in Section 3.5. These treatments included passivation (as-synthesized catalyst), H_2 pretreatment at 400 °C, and increasing periods of exposure (5 min TOS, 10 min TOS, 1 h TOS, and 2 h TOS) to acetic acid and H_2 at 350 °C. The conditions for the acetic acid and H_2 exposure were identical to those used in the acetic acid TPRxn experiments, with the exception that these experiments were isothermal at 350 °C. This temperature was selected because (1) the dominant reaction pathway was hydrogenation-dehydration and (2) it falls within the range of *ex-situ* CFP operating conditions.[4,5] Spectra for Mo 3d, C 1s, and O 1s were collected and are shown in Figure S3. The XPS fit parameters, including peak assignments, peak positions, and FWHM's, are provided in Table S3.

All of the core level spectra were fit with symmetric Gaussian-Lorentzian (80/20) line-shapes. The Mo 3d spectra for the Mo_2C samples were modeled using five doublets. Doublets with Mo $3d_{5/2}$ peaks at 232.9 eV were assigned to MoO_3, corresponding to Mo in the 6+ oxidation state.[9,52-56] Peaks at 229.9 eV were attributed to Mo^{4+}, likely in the form of MoO_2.[9,48,53,55-57] Mo^{2+} $3d_{5/2}$ peaks, corresponding to Mo present in the Mo_2C lattice structure, were observed at 228.4 eV.[48,52,58-60] Additionally, peaks were observed at 231.3 eV and 228.9 eV and were attributed to Mo in 3+ and 5+ oxidation states, respectively, and may correspond to Mo present in the form of an oxycarbide or oxy-carbohydride phase.[9,48,54-57,61] The O 1s spectra were fit with three peaks. Peaks at 230.3 eV were attributed to oxygen present in Mo oxide species,[48,53-55,58] and the peaks at 532.5 eV were assigned to strongly bound O^-, OH^-, H_2O, and O=C.[48,55,62] The peaks at 531.2 eV have tentatively been assigned to oxygen present in Mo

Pursuant to the DOE Public Access Plan, this document represents the authors' peer-reviewed, accepted manuscript. The published version of the article is available from the relevant publisher.

oxycarbide or oxy-carbohydride phases. The C 1s spectra were fit with four peaks, corresponding to carbidic carbon (283.5 eV),[48,58] adventitious carbon (284.4 eV), and species containing C-O (285.6 eV)[48,53,62] and C=O (288.6 eV)[48,53,62] bonds.

As shown in Table 3 and Figure S3, the surface of the as-synthesized, passivated Mo_2C sample was composed primarily of MoO_3 (49% of the surface Mo was present as Mo^{6+}). Only 19% of the surface Mo was present in the form of Mo_2C (Mo^{2+}). The dominant species (75%) in the O 1s spectrum for the passivated sample corresponded to Mo oxides. These results are in good agreement with the calculated O/Mo atomic ratio of 2.26 (Table 3). Similar O/Mo ratios for passivated Mo_2C samples have been reported.[44] Although the surface was heavily oxidized, the carbidic carbon peak still dominated the C 1s spectrum. However, there were also contributions from adventitious carbon and adsorbed species containing C-O and C=O bonds. The atomic ratios for total C/Mo and carbidic C/Mo^{2+} for the passivated sample were 0.61 and 1.20 (Table 3). These ratios suggest that the overall stoichiometry of the sample was consistent with Mo_2C (total C/Mo atomic ratio of 0.5), but that some of the Mo initially present as Mo_2C had been oxidized during passivation to form surface oxides and oxycarbides.

Table 3. Selected atomic ratios determined by XPS for species on the surface of the Mo_2C catalyst following various treatments.

Treatment	C/Mo Atomic Ratio	Carbidic C/Mo^{2+} Atomic Ratio	O/Mo Atomic Ratio	O/C Atomic Ratio
Passivated	0.61	1.20	2.26	3.7
H_2 Pretreated	0.57	0.98	0.82	1.4
5 min TOS	0.80	1.04	0.75	0.93
10 min TOS	0.94	1.13	0.76	0.80
1 h TOS	1.24	1.04	0.83	0.67
2 h TOS	1.34	1.09	0.70	0.53

Pursuant to the DOE Public Access Plan, this document represents the authors' peer-reviewed, accepted manuscript. The published version of the article is available from the relevant publisher.

Following pretreatment in H_2 at 400 °C, the Mo^{6+} contribution was almost completely eliminated and the Mo^{2+} concentration increased to ca. 36%. However, most of the surface Mo is still present in higher oxidation states ($3^+ - 5^+$), suggesting incomplete reduction of the surface. Similarly, the O 1s spectrum for the pretreated sample exhibits a decreased concentration of oxygen present in Mo oxides (41%) and an increase in oxygen present in oxycarbide phases (44%). Additionally, the pretreatment step caused the formation of surface hydroxyls (binding energy of 532.5 eV), consistent with our NH_3-TPD results in which surface acidity was attributed to hydroxyls on the Mo_2C surface. The pretreatment resulted in a decrease in the O/Mo atomic ratio from 2.26 to 0.82, and a reduction in the surface concentration of carbon species containing C-O and C=O bonds.

Under reaction conditions with acetic acid and H_2, minimal changes were observed in the Mo 3d and O 1s spectra as a function of TOS compared to the pretreated sample. Peaks corresponding to the oxycarbide phases (Mo $3^+ - 5^+$ and O 1s 531.2 eV) and surface hydroxyls (O 1s 532.5 eV) persisted throughout the duration of the experiment. The O/Mo atomic ratio fluctuated around the pretreated value, but did not exhibit any trend with TOS. This result suggests that oxygen accumulation (beyond the level of oxygen present following pretreatment) does not occur under these reaction conditions. In contrast, the total C/Mo atomic ratio increased significantly with TOS (Table 3 and Figure S4). From the C 1s spectra in Figure S3, it is clear that the carbon is being deposited in a form similar to adventitious carbon (i.e., C-C bonds, hydrocarbons). This observation is further supported by the minimal change observed in the carbidic C/Mo^{2+} ratios as a function of TOS. This trend in carbon deposition as a function of TOS is similar to that reported by Lee et al. for the hydrodeoxygenation of anisole over Mo_2C.[18]

Pursuant to the DOE Public Access Plan, this document represents the authors' peer-reviewed, accepted manuscript. The published version of the article is available from the relevant publisher.

Carbon deposition has also been reported to be the cause of the initial deactivation of Mo_2C for WGS.[44]

3.5. DFT Calculations

3.5.1. Oxygen Coverage on Mo_2C

Experimental XPS data of the Mo_2C catalyst indicates the presence of substantial surface oxygen, possibly extending 5 nm into the bulk. To determine the most energetically favorable surface coverage of oxygen under the experimental reaction conditions, we constructed two-dimensional phase diagrams of oxygen coverage at varying temperatures and partial pressures of water for the Mo-Mo_2C(001) and C-Mo_2C(001) surfaces. The first step in generating the phase diagrams was identification of the minimum energy configurations of oxygen adsorption and differential binding energies at discrete coverages of 0.25 ML, 0.50 ML, 0.75 ML, 1.00 ML and 1.25 ML (Figure 9). Our results for oxygen coverage as a function of surface coverage and surface termination are generally consistent with previous work by Liu and Rodriguez.[63]

The two dimensional phase diagrams of oxygen coverage at varying temperatures and partial pressures of water relevant to the acetic acid TPRxn experiments for the Mo-Mo_2C(001) and C-Mo_2C(001) surfaces are shown in Figure 10a and 10b, respectively. The experimental TPRxn data for water partial pressure versus temperature, assuming the production of one water molecule for every acetic acid molecule converted, is included on the phase diagrams to enable easy identification of the experimental reaction conditions. When constructing the phase diagrams, the hydrogen partial pressure was held constant at 0.1 atm, equivalent to the H_2 partial pressure in the feed for acetic acid TPRxn. Varying the partial pressure of hydrogen over the range observed experimentally did not lead to significant changes in the phase diagrams.

Pursuant to the DOE Public Access Plan, this document represents the authors' peer-reviewed, accepted manuscript. The published version of the article is available from the relevant publisher.

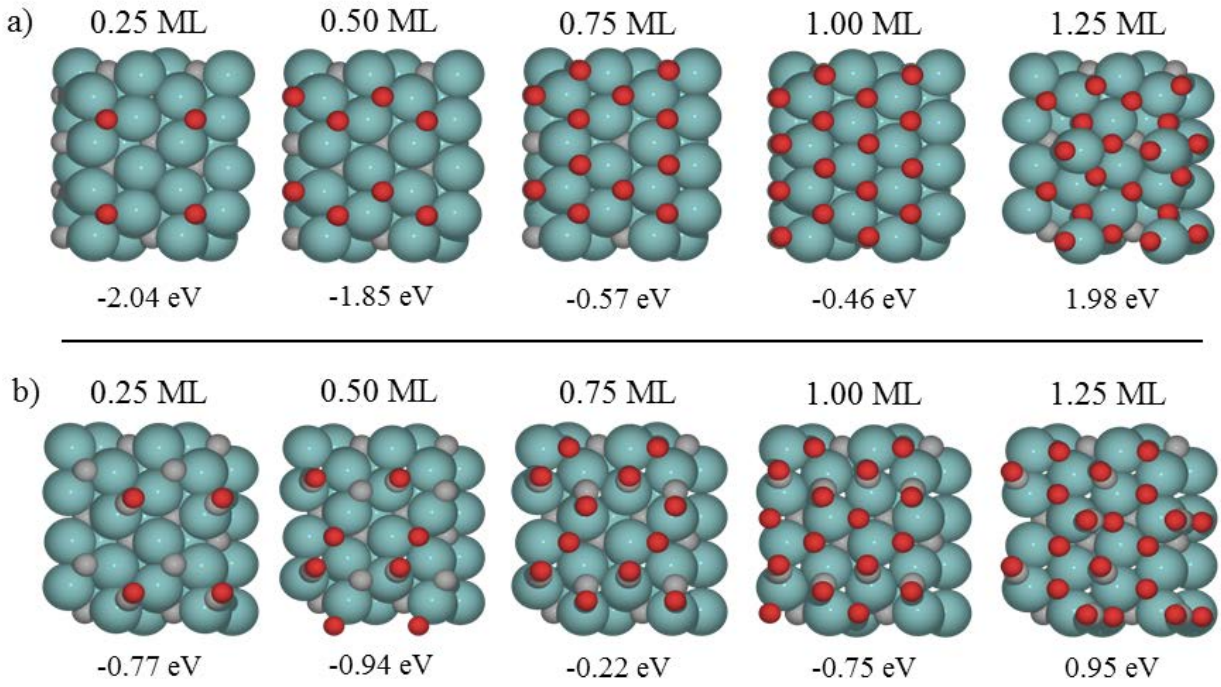

Figure 9. Top views of the minimum energy geometries and differential binding energies for atomic oxygen adsorption at varying coverages on the (a) Mo-Mo_2C(001) and (b) C-Mo_2C(001) surfaces. Calculations were performed using a (1 x 1) unit cell, but (2 x 2) unit cells are shown for clarity. 1 ML of oxygen is defined as 1 O atom per each Mo atom on the Mo-terminated surface and 2 O atoms per one C atom on the C-terminated surface. Red, green and gray spheres represent O, Mo, and C, respectively.

The phase diagrams demonstrate that the minimum energy oxygen-coverage on both the Mo-terminated and C-terminated surfaces is at or near 1 ML at temperatures below ca. 350 °C. As the temperature increases above ca. 350 °C, the most energetically favorable oxygen-coverage on the Mo-terminated and C-terminated surfaces are 0.75 ML and 0.50 ML, respectively. For the C-Mo_2C(001) surface, the most favorable oxygen-coverage remains as 0.50 ML up to 600 °C, whereas the coverage decreases from 0.75 ML to 0.50 ML above ca. 450 °C on the Mo-terminated surface. These phase diagrams are consistent with the minimal change observed in O/Mo ratio by XPS as a function of TOS at 350 °C. We note that these phase diagrams are simplified models and that the surface likely includes subsurface oxygen based on the XPS

Pursuant to the DOE Public Access Plan, this document represents the authors' peer-reviewed, accepted manuscript. The published version of the article is available from the relevant publisher.

results reported; future work will aim to explore the effect of subsurface oxygen. However, the results presented here qualitatively illustrate that the surface coverage of oxygen on Mo-Mo_2C(001) and C-Mo_2C(001), under conditions of acetic acid conversion greater than ca. 20% (i.e., temperatures above ca. 350 °C), is likely significant, but may not reach a full monolayer. Based on these phase diagrams, a sub-monolayer of oxygen was likely present on the Mo_2C surface at the conditions for which maximum production of acetaldehyde (i.e., C-O bond cleavage) was observed during TPRxn experiments (ca. 400 °C), suggesting that O, Mo, and C sites may all be present under reaction conditions.

We also constructed phase diagrams for the two surfaces under typical *ex-situ* CFP conditions.[2-5] For the diagrams shown in Figure 10c and 10d, the temperature was held constant at 350 °C, the hydrogen partial pressure (P_{H2}) was varied from 0 – 5 atm, and the water partial pressure (P_{H2O}) was varied between 0.5 and 2 atm. The range of H_2 partial pressures and H_2O partial pressures were chosen based on the *ex-situ* CFP design cases from Dutta et al.[2,4] At 350 °C, we found that both the Mo-terminated and C-terminated surfaces are predicted to be highly covered in oxygen. We note that the temperature, which is within the typical range of *ex-situ* CFP conditions (300 °C – 500 °C), had a significant impact on the predicted oxygen coverages. At the higher end of the temperature range, oxygen surface coverages of 0.75 ML and 0.50 ML were determined to be more stable on the Mo-terminated and C-terminated surfaces, respectively (Figure S5). The underlying source of differences in the phase diagrams generated for the TPRxn experiments versus realistic *ex-situ* CFP conditions was the water partial pressure: the water pressure in the design case was two orders of magnitude greater than the highest water partial pressures observed during acetic acid TPRxn. We note that in both our acetic acid TPRxn experiments and during *ex-situ* CFP, many other species, in addition to water, are available to

Pursuant to the DOE Public Access Plan, this document represents the authors' peer-reviewed, accepted manuscript. The published version of the article is available from the relevant publisher.

oxygenate the Mo_2C catalyst surface. These phase diagrams, generated based on varying water and H_2 partial pressures, are therefore intended to provide qualitative insight into the propensity of the surfaces toward oxygen incorporation under realistic operating conditions.

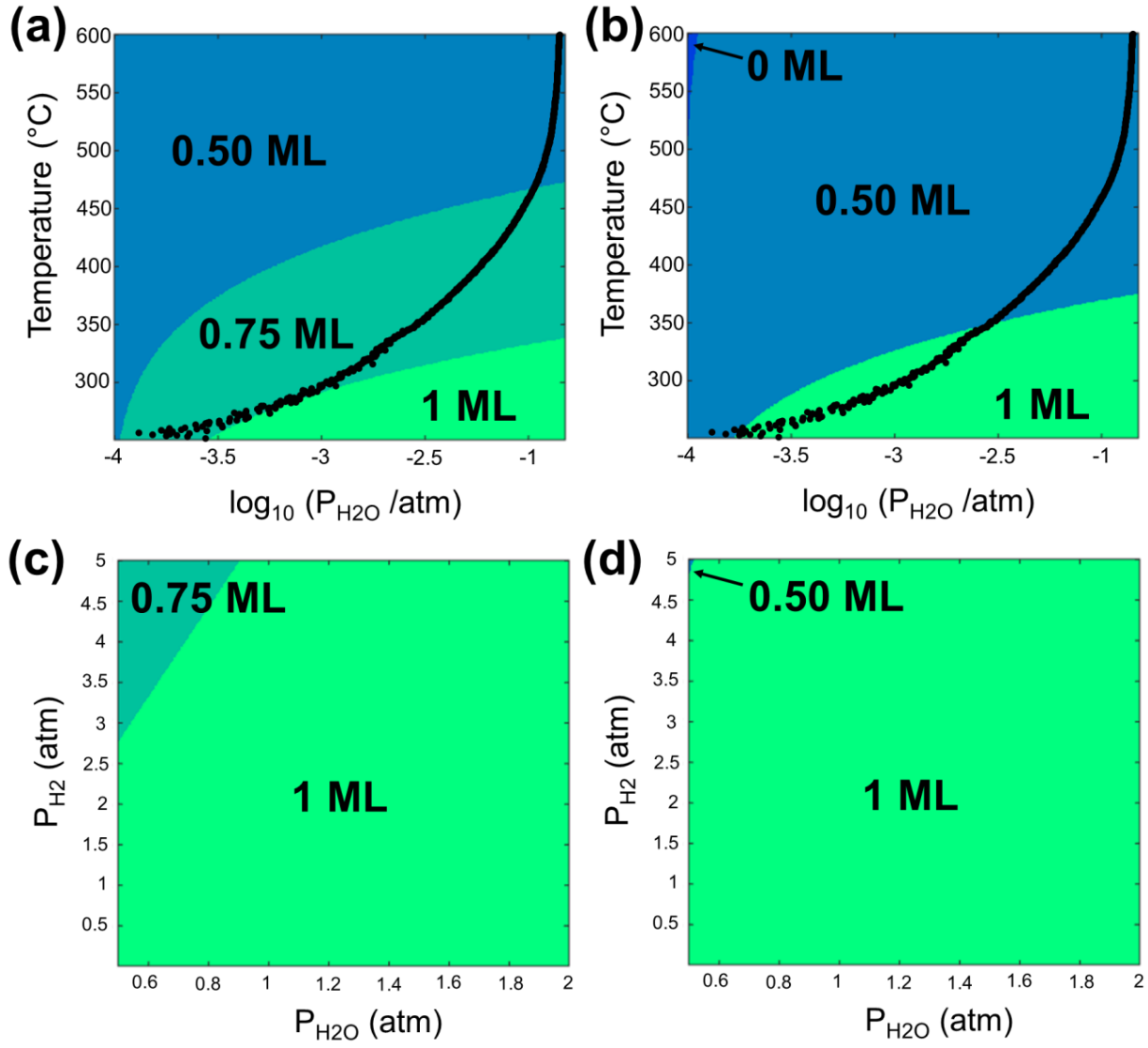

Figure 10. Phase diagrams for atomic oxygen coverage on the (a, c) Mo-Mo_2C(001) and (b, d) C-Mo_2C(001) surfaces. Figures (a) and (b) were generated at a H_2 partial pressure of 0.1 atm and temperatures and water partial pressures representative of the TPRxn experimental conditions. The black points on the plots represent the specific temperature and water partial pressures observed in the TPRxn experiments. Figures (c) and (d) were generated at 350 °C and partial pressures of H_2 and water typical of *ex-situ* CFP conditions. 1 ML of oxygen is defined as 1 O atom per each Mo surface atom on the Mo-terminated surface and 2 O atoms per one C surface atom on the C-terminated surface.

Pursuant to the DOE Public Access Plan, this document represents the authors' peer-reviewed, accepted manuscript. The published version of the article is available from the relevant publisher.

3.5.2. Adsorption of Reactants and Reaction Intermediates

We investigated the adsorption of reaction intermediates that may be involved in steps leading to the production of acetaldehyde from acetic acid based on the experimental DRIFTS and TPRxn results. Based on the results shown in the phase diagrams, we modeled the adsorption of intermediates on the 0.75 ML O/Mo-Mo_2C(001) and 0.50 ML O/C-Mo_2C(001) surfaces. The reported binding energies (BE) of adsorbates on the 0.75 ML O/Mo-Mo_2C(001) were calculated relative to the relaxed 0.75 ML O/Mo-Mo_2C(001) slab ($E_{0.75\ ML\ O/Mo\text{-}Mo2C}$) and the respective adsorbate in the gas phase (E_{gas}) as shown in eq 12:

$$BE = E_{total} - E_{0.75\ ML\ O/Mo\text{-}Mo2C} - E_{gas} \qquad (12)$$

where E_{total} is the total energy of the adsorbed system. The reported binding energies of adsorbates on the 0.50 ML O/C-Mo_2C(001) were calculated analogously.

Table 4 shows the minimum energy adsorption geometry and binding energy for CH_3COOH, CH_3COO, and CH_3CHO on each of the two surfaces considered. Acetic acid binds more strongly to the 0.50 ML O/C-Mo_2C(001) surface, whereas CH_3COO and CH_3CHO bind more strongly to the 0.75 ML O/Mo-Mo_2C(001) surface. On both surfaces, acetic acid prefers to bind in a monodentate configuration, through its C=O, to an oxygen vacancy site (as compared to 1 ML oxygen coverage). The bidentate structure was less stable by 0.54 eV on the 0.75 ML O/Mo-Mo_2C(001) surface. We did not identify a stable bidentate structure on the 0.50 ML O/C-Mo_2C(001) surface. These findings are consistent with DRIFTS results, which showed that monodentate acetic acid bound to Mo on the Mo_2C surface was the preferred adsorption geometry at elevated temperatures and in the presence of an overpressure of acetic acid.

The deprotonation of acetic acid is approximately isoenergetic on the 0.50 ML O/C-Mo_2C(001) surface (ΔE = 0.01 eV) and exothermic on the 0.75 ML O/Mo-Mo_2C(001) surface

Pursuant to the DOE Public Access Plan, this document represents the authors' peer-reviewed, accepted manuscript. The published version of the article is available from the relevant publisher.

with a reaction energy of -0.35 eV. Deprotonation of adsorbed acetic acid (and the formation of C-H and possibly Mo-H bonds) was also observed using DRIFTS. The acetate intermediate prefers a monodentate configuration at a three-fold hollow site on the 0.75 ML O/Mo-Mo_2C(001) surface, but the bidentate configuration is only 0.1 eV less stable. Acetate prefers a bidentate configuration, with both oxygen atoms coordinated to top Mo sites on the 0.50 ML O/C-Mo_2C(001). Two additional acetate configurations had similar stabilities on the 0.50 ML O/C-Mo_2C(001) surface: (1) the bidentate configuration in which one O is coordinated to a top Mo site and one oxygen atom is coordinated to a top C site is only ca. 0.1 eV less stable and (2) a monodentate configuration at a top Mo site is only ca. 0.4 eV less stable than the most stable geometry. Thus, interconversion between the various acetate adsorption geometries is likely facile on both surfaces, in agreement with the DRIFTS results. The adsorption geometry of CH_3CHO is similar on both surfaces, as is the adsorption energy. Comparison of the adsorption modes and binding strengths on the two surfaces illustrates the significant impact both surface termination and oxygen coverage should have on the reaction energetics. Importantly, changes in surface termination and oxygen coverage could ultimately result in completely different reaction pathways under different reaction conditions, namely partial pressures of H_2 and H_2O and reaction temperature.

The binding energies of atomic H at the Mo and O sites on 0.75 ML O/Mo-Mo_2C(001) and at the Mo, O and C sites on 0.50 ML O/C-Mo_2C(001) are reported in Table 5. On the 0.50 ML O/C-Mo_2C(001) surface, H prefers to bind to a C site, suggesting that if an empty C site exists on the C-terminated surface, deprotonation of acetic acid to produce a C-H bond is likely, as observed in the DRIFTS experiments. This result supports the presence of the C-terminated

Pursuant to the DOE Public Access Plan, this document represents the authors' peer-reviewed, accepted manuscript. The published version of the article is available from the relevant publisher.

surface under reaction conditions, and the potential involvement of this surface as the active site for the initial deprotonation step and/or for hydrogenation steps.

Table 4. Binding energies, top views and side views of the minimum energy structures for adsorbates on 0.75 ML O/Mo-Mo_2C(001) and 0.5 ML O/C-Mo_2C(001). All results are calculated on a 2 x 2 surface unit cell. Red, green and gray spheres represent O, Mo, and C in the Mo_2C surface, respectively. White, pink and yellow spheres represent H, O and C in the adsorbed species, respectively.

Adsorbate	0.75 ML O/Mo-Mo_2C(001)			0.50 ML O/C-Mo_2C(001)		
	BE (eV)			BE (eV)		
CH_3COOH	-1.34	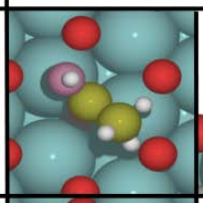	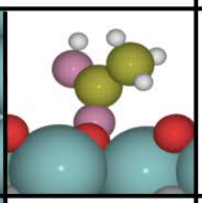	-1.47	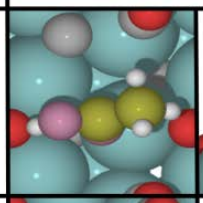	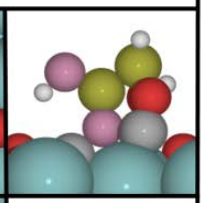
CH_3COO	-3.48	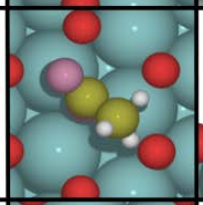	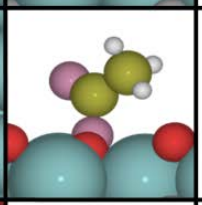	-2.99	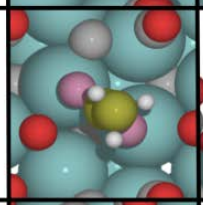	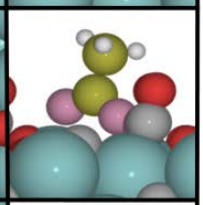
CH_3CHO	-1.56	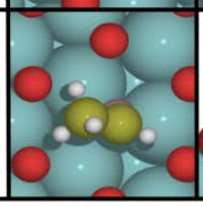	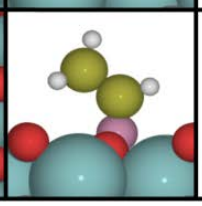	-1.29	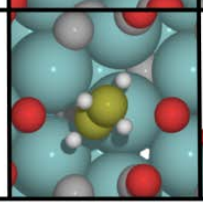	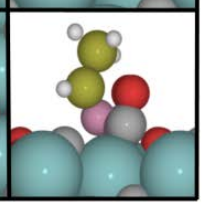

Table 5. Binding energies of atomic H at various adsorption sites on 0.75 ML O/Mo-Mo_2C(001) and 0.5 ML O/C-Mo_2C(001). All results are calculated in a 2 x 2 surface unit cell.

	Site	**Binding Energy (eV)**
0.75 ML O/Mo-Mo_2C(001)		
Mo	hollow	-2.75
O	top	-2.76
0.50 ML O/C-Mo_2C(001)		
Mo	bridge	-2.50
O	top	-2.19
C	top	-3.02

Pursuant to the DOE Public Access Plan, this document represents the authors' peer-reviewed, accepted manuscript. The published version of the article is available from the relevant publisher.

3.5.3. Water Removal on the O-covered Mo-Mo_2C(001) Surface

The preferential adsorption of the reaction intermediates, through their O atoms, at Mo sites and the strong adsorption of oxygen to both surfaces suggests that oxygen vacancy chemistry (as compared to 1 ML O coverage) may be important in the overall reaction mechanism. Thus, we investigated the energetics of removal of an adsorbed surface oxygen atom as water to create a vacancy site on the 1ML O/Mo-Mo_2C(001) surface. The site with the minimum thermochemical energetic cost to create an oxygen vacancy is removal of an oxygen at a three-fold hollow site with a carbidic carbon sitting directly below it in the second layer of the Mo_2C surface. The resulting potential energy surface for this process is shown in Figure 11 and the transition state geometries can be found in Figure S6.

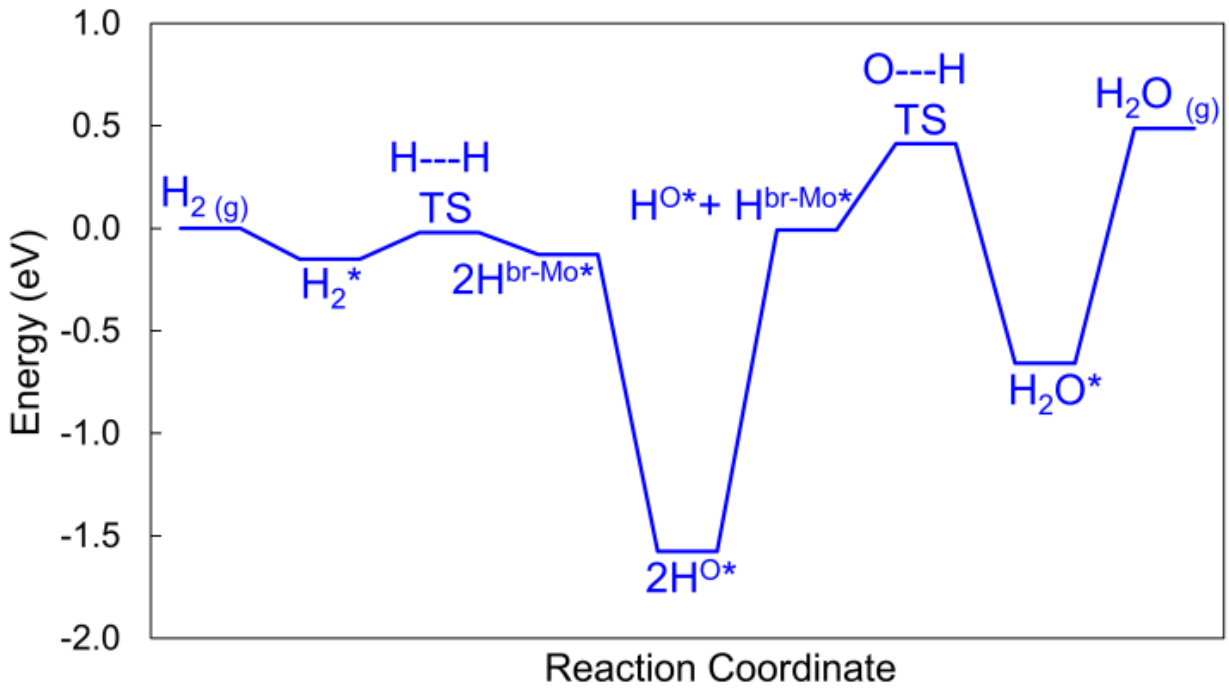

Figure 11. Potential energy surface for oxygen removal to create a vacancy site via H_2O formation on the 1 ML O/Mo-Mo_2C(001) surface. H_2 dissociation was calculated at an oxygen vacancy on the 1 ML O/Mo-Mo_2C(001) surface. * indicates an adsorbed species and superscripts indicate the adsorption site of atomic hydrogen.

Pursuant to the DOE Public Access Plan, this document represents the authors' peer-reviewed, accepted manuscript. The published version of the article is available from the relevant publisher.

H_2 physisorbs to an oxygen vacancy site on the 1 ML O/Mo-Mo_2C(001) surface with a binding energy of -0.15 eV. The initial step, involving H_2 dissociation at the vacancy site on the 1 ML O/Mo-Mo_2C(001) surface to form surface hydroxyls, has a low activation energy barrier (E_A = 0.13 eV), and the overall step is exothermic with a reaction energy of -1.43 eV. The subsequent step requires cleavage of an O-H bond and formation of a second O-H bond at an existing hydroxyl group. The large energy difference (ΔE = 1.57 eV) between the two infinitely separated hydroxyl groups ($2H^{O}$*) and an O bound to a bridge Mo site near one hydroxyl group (H^{O}*+$H^{br\text{-}Mo}$*), is indicative of the strong O-H bonds in the individual hydroxyl groups. The intrinsic barrier for forming the second O-H bond to produce adsorbed water is comparatively low (E_A = 0.42 eV). The following step, desorption of the water molecule, is endothermic (ΔE = 1.14 eV). Comparison of these results with previous theoretical studies of oxygen removal on Mo_2C suggests that the energetics are highly dependent on the oxygen surface coverage.[11,63] Liu and Rodriguez found that water adsorbs to the clean Mo-Mo_2C surface with an adsorption energy of -1.52 eV, whereas it does not adsorb on the 1 ML O-covered surface. Additionally, on the oxygen-covered surface, it was reported that water formation via OH* + H* → H_2O* is exothermic with a reaction energy of -3.39 eV, whereas on the clean Mo-Mo_2C surface, the elementary step is endothermic with a reaction energy of 0.48 eV.[63] Thus, an important factor in determining the kinetics of water removal is the availability of surface hydrogen,[11] such that either (1) the O-H bond strength of the hydroxyl groups decreases at higher hydroxyl coverages or (2) all oxygen sites are occupied by a H, requiring additional hydrogen adsorbates to bind at Mo (or C) sites near hydroxyl groups. These calculations support the high concentration of hydroxyl sites (i.e., acidic sites) on the Mo_2C surface, as titrated by NH_3-TPD. Further, these calculations are consistent with the low extent of observed hydrogenation during acetic acid and

Pursuant to the DOE Public Access Plan, this document represents the authors' peer-reviewed, accepted manuscript. The published version of the article is available from the relevant publisher.

ethanol TPRxn, and suggest that H_2O removal may be a kinetically limiting step due to a lack of available adsorbed H.

3.5.4. Acidity of Hydroxyl Groups

We have discussed that the surface of the Mo_2C catalyst, regardless of termination, contains a significant coverage of atomic oxygen and that this oxygen forms strong bonds with hydrogen atoms. Others have also reported the formation of surface hydroxyls on Mo_2C that act as Brønsted acid sites.[9] Thus, the acidity of these surface hydroxyls was probed on the 0.75 ML O/Mo-Mo_2C(001) and 0.5 ML O/C-Mo_2C(001) surfaces by calculating NH_3 adsorption energies. Hibbitts et al. have previously reported the correlation between DFT-calculated NH_3 adsorption energy and deprotonation energy,[42] though we note that the use of NH_3 adsorption energies for comparisons of acid site strength is the subject of ongoing debate.[64]

The results of the NH_3 adsorption calculations, including N-H and O-H bond distances, are reported in Table 6. Two possible hydroxyl sites exist on the Mo-terminated surface: OH groups at hollow sites above a carbidic C in the second layer and OH groups at hollow sites where the carbidic C is in the fourth layer. We refer to these sites as OH site A and OH site B, respectively. A hydroxyl on the 0.5 ML O/C-Mo_2C(001) surface was found to be more acidic (i.e., stronger NH_3 adsorption energy) than either hydroxyl on the 0.75 ML O/Mo-Mo_2C(001). Interestingly, these NH_3 adsorption energies can be compared with the adsorption energies of NH_3 on a variety of zeolites determined using density functional theory[65,66] and microcalorimetry,[67] for a qualitative comparison of the acidity of hydroxyls on Mo_2C with Brønsted acid sites on common zeolites. The NH_3 adsorption energies at hydroxyl sites on 0.50 ML O/C-Mo_2C(001) and on 0.75 ML O/Mo-Mo_2C(001) are comparable to the NH_3 adsorption energies reported for H-Beta, H-Y, and H-X zeolites. As shown for Mo_2C in this work, H-Beta, H-Y, and H-X zeolites have been

Pursuant to the DOE Public Access Plan, this document represents the authors' peer-reviewed, accepted manuscript. The published version of the article is available from the relevant publisher.

reported to be active for ethanol dehydration to ethylene over the temperature range 250-400°C,[68,69] suggesting that surface hydroxyls on Mo_2C may play a role in the catalytic deoxygenation of acetic acid.

Table 6. Binding energies, N-H and O-H bond distances for NH_3 adsorption at hydroxyl sites on 0.75 ML O/Mo-Mo_2C(001) and 0.5 ML O/C- Mo_2C(001). The N-H bond distance is the distance between the N in NH_3 and the H in the hydroxyl group. All results are calculated in a 2 x 2 surface unit cell.

	NH_3 Adsorption Energy (eV)	**N-H Distance (Å)**	**O-H Distance (Å)**
0.75 ML O/Mo-Mo_2C(001), OH site A	-0.91	1.46	1.08
0.75 ML O/Mo-Mo_2C(001), OH site B	-1.15	1.25	1.22
0.50 ML O/C-Mo_2C(001)	-1.35	1.14	1.40

3.6. Reaction Pathways and Active Site Interpretations

The experimental and computational results presented within this work suggest that the Mo_2C surface was at least partially covered with oxygen under reaction conditions and that multiple types of sites were present, including Brønsted acidic hydroxyl sites, exposed Mo sites (i.e., oxygen vacancy sites as compared to 1 ML oxygen coverage), and C sites. The relative concentration of these sites is a function of the reaction conditions, namely temperature, H_2 partial pressure, and H_2O partial pressure. The conversion of acetic acid over Mo_2C produced primarily acetaldehyde and ethylene at temperatures below 400 °C, most likely proceeding through an ethoxy intermediate. This deoxygenation pathway cleaves C-O bonds and requires both deoxygenation/dehydration and hydrogenation sites. The deoxygenation/dehydration sites may be (1) the acidic surface hydroxyls similar in nature to Brønsted acid sites on zeolites and/or (2) surface oxygen vacancies (exposed Mo sites) capable of direct deoxygenation, possibly through a reverse Mars-van Krevelen mechanism, in a similar fashion to that proposed for MoO_3

Pursuant to the DOE Public Access Plan, this document represents the authors' peer-reviewed, accepted manuscript. The published version of the article is available from the relevant publisher.

by Prasomsri et al.[70] The role of the vacancy sites in deoxygenation is supported by the DRIFTS results, which showed the formation of Mo-O/Mo-OH bonds upon reaction of acetic acid. The hydrogenation sites are proposed to be either exposed Mo sites or C sites, as evidenced from the formation of C-H bonds during H_2 reduction and upon deprotonation of adsorbed acetic acid. Based on our findings that (1) C-H bonds form upon surface reduction (DRIFTS), (2) acidic sites cover approximately 40% of the catalyst surface following pretreatment (NH_3-TPD), and (3) acetate prefers a bidendate adsorption geometry (DRIFTS and DFT calculations), it is proposed that the 0.50 ML O/C-Mo_2C(001) model surface most closely resembles the working catalyst surface under the reaction conditions used in this study.

For acetic acid deoxygenation over Mo_2C below 400 °C, C-O cleavage steps (i.e., ethanol dehydration) appeared to be relatively facile compared to hydrogenation steps (i.e., acetaldehyde hydrogenation to ethanol). It is expected that the hydrogenation of surface bound intermediates and removal of surface oxygen as H_2O (regenerating the O-vacancy site) would be strong functions of hydrogen availability. Based on H_2 chemisorption, the Mo_2C surface possessed a low density of metallic-like H-adsorption sites following reduction at 400 °C. These findings highlight the need to balance the density and relative strengths of metallic-like hydrogenation sites and acidic/oxygen vacancy sites on the Mo_2C surface, and optimize reaction conditions in order to further enhance deoxygenation.

4. CONCLUSION

The surface chemistry, active site identity, and deoxygenation pathways of Mo_2C under *ex-situ* CFP conditions were probed through the conversion of acetic acid, a model compound representative of carboxylic acids present in biomass pyrolysis vapors. The Mo_2C surface was

Pursuant to the DOE Public Access Plan, this document represents the authors' peer-reviewed, accepted manuscript. The published version of the article is available from the relevant publisher.

found to remain partially oxidized following pretreatment and under reaction conditions, potentially existing as an oxycarbide, and this partially oxidized surface possessed metallic-like H-adsorption sites, oxygen vacancy sites (exposed Mo sites), and acidic sites. The metallic-like H-adsorption sites were attributed to exposed C and Mo sites, and the acidic sites were attributed to surface hydroxyls, which were present at a density 8 times greater than the metallic-like sites following pretreatment. Based on calculated NH_3 adsorption energies, the strength of these acidic sites was similar to Brønsted sites present on H-Beta, H-Y, and H-X zeolites. Below 400 °C, the Mo_2C catalyst favored cleavage of C-O bonds over C-C bonds producing primarily acetaldehyde and ethylene, likely proceeding through a pathway including an ethoxy intermediate. It is proposed that these C-O cleavage steps proceed over either the acidic hydroxyl sites or oxygen vacancy (exposed Mo) sites. The hydrogenation of surface-bound intermediates was limited due to the low density of metallic-like H-adsorption sites on the Mo_2C surface, thus resulting in a product mixture favoring acetaldehyde instead of ethylene/ethane. The reactivity of the carbide surface varied considerably with temperature, shifting from C-O cleavage at temperatures below 400 °C to decarbonylation and decarboxylation (C-C cleavage) at temperatures above 400 °C. Based on calculated phase diagrams, the relative concentrations of the different types of sites also vary considerably as a function of reaction conditions, namely temperature and partial pressures of H_2 and H_2O. The results from this work indicate that Mo_2C, and transition metal carbides in general, are promising catalysts for *ex-situ* CFP of biomass due to their oxophilic nature and bifunctional properties. Enhanced deoxygenation and increased hydrogen incorporation may be achievable through tailoring the density, availability, and relative strengths of the metallic-like H-adsorption sites, acidic hydroxyl sites, and oxygen vacancy sites.

Pursuant to the DOE Public Access Plan, this document represents the authors' peer-reviewed, accepted manuscript. The published version of the article is available from the relevant publisher.

ASSOCIATED CONTENT

Supporting Information. Experimental details for mass spectra deconvolution (Tables S1 and S2), H_2 temperature programmed reduction of Mo_2C (Figure S1), temperature-dependent DRIFTS spectra (Figure S2), XPS fit parameters (Table S3) and spectra (Figure S3), C/Mo atomic ratios for Mo_2C as a function of TOS (Figure S4), phase diagrams for atomic oxygen coverage on Mo-Mo_2C(001) and C-Mo_2C(001) surfaces (Figure S5), and transition state structures for H_2 dissociation and water formation on the 1 ML O/Mo-Mo_2C(001) surface (Figure S6) are provided in the Supporting Information. This material is available free of charge via the Internet at http://pubs.acs.org.

AUTHOR INFORMATION

Corresponding Author

*E-mail: Joshua.Schaidle@nrel.gov

Notes

The authors declare no competing financial interests.

ACKNOWLEDGMENT

This work was supported by the Laboratory Directed Research and Development Program at the National Renewable Energy Laboratory and the Department of Energy Bioenergy Technologies Office under Contract no. DE-AC36-08-GO28308. The authors would also like to thank Mayank Behl for performing the NH_3-TPD experiments. The U.S. Government retains and the publisher, by accepting the article for publication, acknowledges that the U.S. Government retains a nonexclusive, paid up, irrevocable, worldwide license to publish or reproduce the published form of this work, or allow others to do so, for U.S. Government purposes.

Pursuant to the DOE Public Access Plan, this document represents the authors' peer-reviewed, accepted manuscript. The published version of the article is available from the relevant publisher.

REFERENCES

(1) *Multi-Year Program Plan*, U. S. Department of Energy Bioenergy Technologies Office, 2015.

(2) Dutta, A.; Sahir, A.; Tan, E.; Humbird, D.; Snowden-Swan, L. J.; Meyer, P.; Ross, J.; Sexton, D.; Yap, R.; Lukas, J. *Process Design and Economics for the Conversion of Lignocellulosic Biomass to Hydrocarbon Fuels: Thermochemical Research Pathways with In Situ and Ex Situ Upgrading of Fast Pyrolysis Vapors*, NREL/TP-5100-62455, NREL, 2015.

(3) Biddy, M.; Dutta, A.; Jones, S.; Meyer, A. *Ex-situ Catalytic Fast Pyrolysis Technology Pathway*, NREL/TP-5100-58050, NREL, 2013.

(4) Dutta, A.; Schaidle, J. A.; Humbird, D.; Baddour, F. G.; Sahir, A. *Top. Catal.* **2015** [Online early access]. DOI: 10.1007/s11244-015-0500-z.

(5) Ruddy, D. A.; Schaidle, J. A.; Ferrell Iii, J. R.; Wang, J.; Moens, L.; Hensley, J. E. *Green Chem.* **2014**, *16*, 454-490.

(6) Bej, S. K.; Bennett, C. A.; Thompson, L. T. *Appl. Catal., A* **2003**, *250*, 197-208.

(7) Bej, S. K.; Thompson, L. T. *Appl. Catal., A* **2004**, *264*, 141-150.

(8) Zhang, W.; Zhang, Y.; Zhao, L.; Wei, W. *Energy Fuels* **2010**, *24*, 2052-2059.

(9) Sullivan, M. M.; Held, J. T.; Bhan, A. *J. Catal.* **2015**, *326*, 82-91.

(10) Han, J.; Duan, J.; Chen, P.; Lou, H.; Zheng, X.; Hong, H. *Green Chem.* **2011**, *13*, 2561-2568.

(11) Ren, H.; Yu, W.; Salciccioli, M.; Chen, Y.; Huang, Y.; Xiong, K.; Vlachos, D. G.; Chen, J. G. *ChemSusChem* **2013**, *6*, 798-801.

Pursuant to the DOE Public Access Plan, this document represents the authors' peer-reviewed, accepted manuscript. The published version of the article is available from the relevant publisher.

(12) Ren, H.; Chen, Y.; Huang, Y.; Deng, W.; Vlachos, D. G.; Chen, J. G. *Green Chem.* **2014**, *16*, 761-769.

(13) Xiong, K.; Lee, W.-S.; Bhan, A.; Chen, J. G. *ChemSusChem* **2014**, *7*, 2146-2149.

(14) Kelly, T. G.; Chen, J. G. *Green Chem.* **2014**, *16*, 777-784.

(15) Xiong, K.; Yu, W.; Chen, J. G. *Appl. Surf. Sci.* **2014**, *323*, 88-95.

(16) Yu, W.; Mellinger, Z. J.; Barteau, M. A.; Chen, J. G. *J. Phys. Chem. C* **2012**, *116*, 5720-5729.

(17) Lee, W.-S.; Wang, Z.; Wu, R. J.; Bhan, A. *J. Catal.* **2014**, *319*, 44-53.

(18) Lee, W.-S.; Kumar, A.; Wang, Z.; Bhan, A. *ACS Catal.* **2015**, 4104-4114.

(19) Milne, T.; Agblevor, F.; Davis, M.; Deutch, S.; Johnson, D. *Developments in Thermal Biomass Conversion*; Brackie Academic and Professional: London, U.K., 1997.

(20) Patt, J.; Moon, D.; Phillips, C.; Thompson, L. *Catal. Lett.* **2000**, *65*, 193-195.

(21) Schweitzer, N. M.; Schaidle, J. A.; Ezekoye, O. K.; Pan, X.; Linic, S.; Thompson, L. T. *J. Am. Chem. Soc.* **2011**, *133*, 2378-2381.

(22) Wang, G.; Schaidle, J. A.; Katz, M. B.; Li, Y.; Pan, X.; Thompson, L. T. *J. Catal.* **2013**, *304*, 92-99.

(23) Seah, M. P. *Surf. Interface Anal.* **1989**, *14*, 488.

(24) Jensen, C. M.; Lee, D. W. *J. Chem. Educ.* **2000**, *77*, 629.

(25) Ko, E. I.; Benziger, J. B.; Madix, R. J. *J. Catal.* **1980**, *62*, 264-274.

(26) Zhang, Q.; Alfarra, M. R.; Worsnop, D. R.; Allan, J. D.; Coe, H.; Canagaratna, M. R.; Jimenez, J. L. *Environ. Sci. Technol.* **2005**, *39*, 4938-4952.

(27) Kresse, G.; Hafner, J. *Phys. Rev. B* **1993**, *47*, 558.

(28) Kresse, G.; Hafner, J. *Phys. Rev. B* **1994**, *49*, 14251.

Pursuant to the DOE Public Access Plan, this document represents the authors' peer-reviewed, accepted manuscript. The published version of the article is available from the relevant publisher.

(29) Kresse, G.; Furthmüller, J. *Phys. Rev. B* **1996**, *54*, 11169.

(30) Kresse, G.; Furthmüller, J. *Comput. Mater. Sci.* **1996**, *6*, 15-50.

(31) Blöchl, P. E. *Phys. Rev. B* **1994**, *50*, 17953.

(32) Kresse, G.; Joubert, D. *Phys. Rev. B* **1999**, *59*, 1758.

(33) Perdew, J. P.; Burke, K.; Ernzerhof, M. *Phys. Rev. Lett.* **1996**, *77*, 3865.

(34) Perdew, J. P.; Burke, K.; Ernzerhof, M. *Phys. Rev. Lett.* **1997**, *78*, 1396.

(35) Tkatchenko, A.; Scheffler, M. *Phys. Rev. Lett.* **2009**, *102*, 073005.

(36) Monkhorst, H. J.; Pack, J. D. *Phys. Rev. B* **1976**, *13*, 5188-5192.

(37) Parthe, E.; Sadogopan, V. *Acta Crystallogr.* **1963**, *16*, 202-205.

(38) Reuter, K.; Scheffler, M. *Phys. Rev. B* **2001**, *65*, 035406.

(39) Greeley, J.; Mavrikakis, M. *Surf. Sci.* **2003**, *540*, 215-229.

(40) Henkelman, G.; Jonsson, H. *J. Chem. Phys.* **2000**, *113*, 9978-9985.

(41) Satterfield, C. N. *Heterogeneous catalysis in industrial practice,* 2nd ed.; McGraw Hill Book Co.: New York, 1991.

(42) Hibbitts, D.; Tan, Q.; Neurock, M. *J. Catal.* **2014**, *315*, 48-58.

(43) Rachmady, W.; Vannice, M. A. *J. Catal.* **2000**, *192*, 322-334.

(44) Schaidle, J. A.; Lausche, A. C.; Thompson, L. T. *J. Catal.* **2010**, *272*, 235-245.

(45) Claridge, J. B.; York, A. P. E.; Brungs, A. J.; Marquez-Alvarez, C.; Sloan, J.; Tsang, S. C.; Green, M. L. H. *J. Catal.* **1998**, *180*, 85-100.

(46) Nash, C. P.; Ramanathan, A.; Ruddy, D. A.; Behl, M.; Gjersing, E.; Griffin, M.; Zhu, H.; Subramaniam, B.; Schaidle, J. A.; Hensley, J. E. *Appl. Catal., A* **2015**, in press.

(47) Happel, J.; Chao, J. C.; Mezaki, R. *J. Chem. Eng. Data* **1974**, *19*, 110-112.

(48) Cho, H.-G.; Andrews, L. *J. Am. Chem. Soc.* **2005**, *127*, 8226-8231.

Pursuant to the DOE Public Access Plan, this document represents the authors' peer-reviewed, accepted manuscript. The published version of the article is available from the relevant publisher.

(49) Flaherty, D. W.; Berglund, S. P.; Mullins, C. B. *J. Catal.* **2010**, *269*, 33-43.

(50) Tsilomelekis, G.; Boghosian, S. *J. Phys. Chem. C* **2010**, *115*, 2146-2154.

(51) Xu, C.; Goodman, D. W. *J. Phys. Chem.* **1996**, *100*, 1753-1760.

(52) Cheekatamarla, P. K.; Thomson, W. J. *Appl. Catal., A* **2005**, *287*, 176-182.

(53) Delporte, P.; Meunier, F. d. r.; Pham-Huu, C.; Vennegues, P.; Ledoux, M. J.; Guille, J. *Catal. Today* **1995**, *23*, 251-267.

(54) Wei, Z. B. Z.; Grange, P.; Delmon, B. *Appl. Surf. Sci.* **1998**, *135*, 107-114.

(55) Choi, J. G.; Thompson, L. T. *Appl. Surf. Sci.* **1996**, *93*, 143-149.

(56) Prasomsri, T.; Shetty, M.; Murugappan, K.; Roman-Leshkov, Y. *Energy Environ. Sci.* **2014**, *7*, 2660-2669.

(57) Katrib, A.; Leflaive, P.; Hilaire, L.; Maire, G. *Catal. Lett.* **1996**, *38*, 95-99.

(58) St. Clair, T. P.; Oyama, S. T.; Cox, D. F.; Otani, S.; Ishizawa, Y.; Lo, R.-L.; Fukui, K.-i.; Iwasawa, Y. *Surf. Sci.* **1999**, *426*, 187-198.

(59) Mamède, A. S.; Giraudon, J. M.; Löfberg, A.; Leclercq, L.; Leclercq, G. *Appl. Catal., A* **2002**, *227*, 73-82.

(60) Ledoux, M. J.; Huu, C. P.; Guille, J.; Dunlop, H. *J. Catal.* **1992**, *134*, 383-398.

(61) Perez-Romo, P.; Potvin, C.; Manoli, J. M.; Chehimi, M. M.; Djéga-Mariadassou, G. *J. Catal.* **2002**, *208*, 187-196.

(62) Bou, M.; Martin, J. M.; Le Mogne, T.; Vovelle, L. *Appl. Surf. Sci.* **1991**, *47*, 149-161.

(63) Liu, P.; Rodriguez, J. A. *J. Phys. Chem. B* **2006**, *110*, 19418-19425.

(64) Jones, A.; Iglesia, E. *ACS Catal.* **2015**, 5, 5741-5755.

(65) Suzuki, K.; Noda, T.; Sastre, G.; Katada, N.; Niwa, M. *J. Phys. Chem. C* **2009**, 113, 5672-5680.

Pursuant to the DOE Public Access Plan, this document represents the authors' peer-reviewed, accepted manuscript. The published version of the article is available from the relevant publisher.

(66) Agarwal, V.; Metiu, H. *J. Phys. Chem. C* **2015**, 119, 16106-16114.

(67) Auroux, A. *Top. Catal.* **2002**, *19*, 205-213.

(68) Takahara, I.; Saito, M.; Inaba, M.; Murata, K. *Catal. Lett.* **2005**, *105*, 249-252.

(69) Madeira, F. F.; Gnep, N. S.; Magnoux, P.; Maury, S.; Cadran, N. *Appl. Catal., A* **2009**, *367*, 39-46.

(70) Prasomsri, T.; Nimmanwudipong, T.; Roman-Leshkov, Y. *Energy Environ. Sci.* **2013**, *6*, 1732-1738.

Pursuant to the DOE Public Access Plan, this document represents the authors' peer-reviewed, accepted manuscript. The published version of the article is available from the relevant publisher.

TOC Graphic

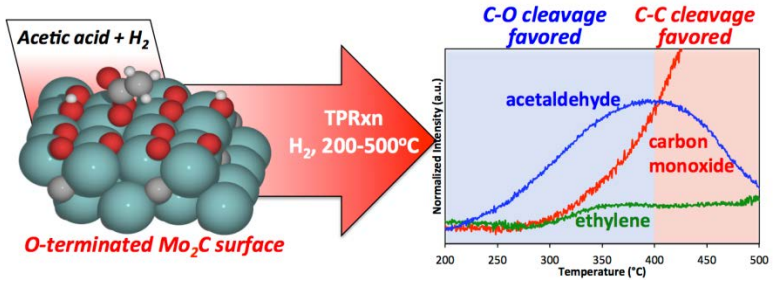

Pursuant to the DOE Public Access Plan, this document represents the authors' peer-reviewed, accepted manuscript. The published version of the article is available from the relevant publisher.